Targeting TGF-β1/miR-21 Pathway in Keratinocytes Reveals Protective Effects of Silymarin on Imiquimod-Induced Psoriasis Mouse Model

Elodie Henriet, Florence Abdallah, Yoan Laurent, Cyril Guimpied, Emily Clement, Michel Simon, Chantal Pichon, Patrick Baril

Targeting TGF-β1/miR-21 Pathway in Keratinocytes Reveals Protective Effects of Silymarin on Imiquimod-Induced Psoriasis Mouse Model

Elodie Henriet[1,2], Florence Abdallah[1,2], Yoan Laurent[1,2], Cyril Guimpied[1,2], Emily Clement[3], Michel Simon[3], Chantal Pichon[1,2] and Patrick Baril[1,2]

Epidermal cells integrate multiple signals that activate the signaling pathways involved in skin homeostasis. TGF-β1 signaling pathway upregulates microRNA (miR)-21-5p in keratinocytes and is often deregulated in skin diseases. To identify the bioactive compounds that enable to modulate the TGF-β1/miR-21-5p signaling pathway, we screened a library of medicinal plant extracts using our miR-ON RILES luciferase reporter system placed under the control of the miR-21-5p in keratinocytes treated with TGF-β1. We identified silymarin, a mixture of flavonolignans extracted from *Silybum marianum* (L.) Gaertn., as the most potent regulator of miR-21-5p expression. Using Argonaute 2 immunoprecipitation and RT-qPCR, we showed that silymarin regulates the expression of miR-21-5p through a noncanonical TGF-β1 signaling pathway, whereas RNA-sequencing analysis revealed three unexpected transcriptomic signatures associated with keratinocyte differentiation, cell cycle, and lipid metabolism. Mechanistically, we demonstrated that SM blocks cell cycle progression, inhibits keratinocyte differentiation through repression of Notch3 expression, stimulates lipid synthesis via activation of PPARγ signaling and inhibits inflammatory responses by suppressing the transcriptional activity of NF-κB. We finally showed that topical application of silymarin alleviates the development of imiquimod-induced psoriasiform lesions in mice by abrogating the altered expression levels of markers involved in inflammation, proliferation, differentiation, and lipid metabolism.

JID Innovations (2023);**3:**100175 doi:10.1016/j.xjidi.2022.100175

INTRODUCTION

As the outermost layer of the skin, the epidermis serves as a physical barrier between the host's body and its environment. It protects against dehydration, harmful microorganisms, UVR, toxic agents, and mechanical insults (Yousef et al., 2022). Keratinocytes (KCs), the predominant cell type of the epidermis, are essential for maintaining epidermal homeostasis and skin repair after injury. KCs originate from quiescent epidermal stem cells that give rise to transient amplifying cells, which then undergo a terminal differentiation program leading to a unique type of programmed cell death, called cornification (Blanpain and Fuchs, 2006; Gonzales and Fuchs, 2017). As KCs move up through the different epidermal layers, they synthesize specific structural and catalytic proteins, including keratins, involucrin (IVL), loricrin (LOR), and transglutaminases, to form the cornified envelope (Candi et al., 2005) as well as lipids to ensure skin barrier function (Smeden van and Bouwstra, 2016).

Signaling molecules such as cytokines, growth factors, and hormones participate in the physiological functions of KCs and contribute to the maintenance of cutaneous homeostasis and epidermal barrier (Guan et al., 2021; Iversen et al., 2005). Among those, TGF-β1 plays a central role in regulating KCs proliferation, differentiation, and migration (Buschke et al., 2011; Jeong and Kim, 2004; Massagué, 2012; Sellheyer et al., 1993). Binding of TGF-β1 to TGF-β type II receptor promotes the recruitment of TGF-β type I receptor and its phosphorylation. Activated TGF-β type I receptor triggers intracellular signaling through phosphorylation of the receptor-mediated SMADs (SMAD2 and SMAD3), which in turn form complexes with the common SMAD, SMAD4 (Massagué, 1998). The activated SMAD2/3−SMAD4 complexes translocate into the nucleus where they regulate the transcription of specific target genes, such as *p21* and *c-myc* to induce G1-phase cell cycle arrest (Frederick et al., 2004; Pardali et al., 2000), *uPA* to promote cell migration (Kocic et al., 2012), and *MAB21L4* to trigger KC differentiation

[1]*Centre de Biophysique Moléculaire, CNRS UPR4301, Orléans, France;* [2]*Unité de Formation et de Recherche, Sciences et Techniques, Université d'Orléans, Orléans, France; and* [3]*Toulouse Institute for Infectious and Inflammatory Diseases (INFINITy), CNRS, INSERM, Toulouse III Paul Sabatier University, Toulouse, France*

Correspondance : Patrick Baril, Centre de Biophysique Moléculaire, CNRS UPR4301, Rue Charles Sadron CS 80054, 45071 Orléans Cedex 2, France E-mail: patrickbaril01@hotmail.com

Abbreviations: AMPK, AMP-activated protein kinase; DEG, differentially expressed gene; HC, high calcium; IMQ, imiquimod; IVL, involucrin; K, keratin; KC, keratinocyte; LOR, loricrin; miR, microRNA; P-body, processing body; PPAR, peroxisome proliferator–activated receptor; RISC, RNA-induced silencing complex; RNA-seq, RNA-sequencing; RT, room temperature; SM, silymarin

Received 14 June 2022; revised 10 November 2022; accepted 11 November 2022; accepted manuscript published online 16 December 2022; corrected proof published online 17 March 2023

Cite this article as: JID Innovations 2023;3:100175

(Ogami et al., 2022). Alternatively, TGF-β1 activates many other downstream signaling pathways such as MAPK, c-Jun N-terminal kinase, extracellular signal–regulated kinase, phosphoinositide-3 kinase/protein kinase B, and RhoA to regulate the epithelial–mesenchymal transition (Bhowmick et al., 2001; Davies et al., 2005; Santibañez, 2006; Santibáñez et al., 2000; Secker et al., 2008). Accumulated evidence indicates that microRNA (miR)-21-5p plays an important role in TGF-β1 signaling in KCs (Wang et al., 2016, 2012; Yang et al., 2011). TGF-β1 upregulates miR-21-5p expression through transcriptional and post-transcriptional mechanisms involving the interaction of receptor-regulated SMADs with the RNA helicase p68 (Davis et al., 2010, 2008). Overexpression of miR-21-5p enhances KCs proliferation and migration by targeting PTEN, PDCD4, and TIMP3 (Wang et al., 2020, 2012; Yan et al., 2016; Yang et al., 2011) and negatively regulates the G1-to-S phase transition through the downregulation of CDC25A associated with cyclin-dependent kinase 2 activation (Wang et al., 2009). In addition to its roles in tissue remodeling (Xie et al., 2022), miR-21-5p plays also essential roles in regulating skin inflammation (Guinea-Viniegra et al., 2014; Liechty et al., 2020; Sonkoly et al., 2008). For instance, Sonkoly et al. (2007) showed that miR-21-5p is one of the most highly expressed miRs in lesional skin and epidermal KCs of patients with psoriasis (Meisgen et al., 2012). Guinea-Viniegra et al. (2014) showed that impaired activation of IL-6/signal transducer and activator of transcription 3 pathway in epidermal lesions of patients with psoriasis could trigger the upregulation of miR-21-5p, which in turn leads to activation of TACE/ADAM17. In line with these studies, we recently identified IL-22 as a potent inducer of miR-21-5p expression (Abdallah et al., 2021) and showed that the passenger miR-21-3p strand, in addition to the mature miR-21-5p strand, positively regulates KC proliferation through the upregulation of cyclin D1. Interestingly, Wang et al. (2020) reported that local delivery of miR-21-5p mimics in excisional wounds of mice accelerates wound healing by promoting re-epithelialization and collagen deposition. Therefore, TGF-β1/miR-21-5p signaling pathway represents a suitable target to search for novel modulators of epidermal homeostasis with possible applications in the management of skin disorders.

Medicinal plants have been proven as a valuable source of bioactive compounds for drug discovery, as evidenced by the fact that nowadays >60% of available drugs are plant-derived natural products or their derivatives (Atanasov et al., 2021; Newman and Cragg, 2020; Salmerón-Manzano et al., 2020). Recent studies have shown that natural products can regulate the expression and processing of miRs, resulting in profound changes in the expression pattern of their target genes involved in multiple signaling pathways (Lin et al., 2017; Zhang et al., 2020). For example, sanguinarine, a bioactive alkaloid extracted from *Sanguinaria canadensis*, has been shown to induce cell cycle arrest and apoptosis in hepatocellular carcinoma cell lines by increasing miR-16.2 promoter occupancy through a p53 mechanism of action (Zhang et al., 2019). Enoxolone, a pentacyclic triterpenoid from the roots of *Glycyrrhiza glabra* exerts antitumor activity through the induction of miR-200c (Hagiwara et al., 2015). Nevertheless, and to our best knowledge, no cellular screening assays have been deployed to identify bioactive structures as regulators of miR expression in the context of cutaneous biology. In this study, we employed the RILES miR-ON reporter assay to identify such compounds. The RILES technology relies on an engineered genetic expression system to switch-ON the expression of reporter genes as Luciferase (Ezzine et al., 2013), hNIS (Simion et al., 2017), or GFP (Simion et al., 2021) when a miR of interest is functionally expressed in cells. We showed that unlike qRT-PCR method, the RILES system offers the opportunity to shed light on the dynamic regulation of miRs in biological processes, resulting in a better understanding of the molecular basis of disease as well as the development of optimized therapeutic strategies (Ezzine et al., 2013; Simion et al., 2021, 2020). In addition to these advantages, we also reported that the RILES system possesses attributes to be used as a miR cellular screening platform to identify novel miR modulators (Simion et al., 2021).

In this study, we asked whether screening a medicinal plant extracts library with the miR-ON RILES reporter system placed under the control of the TGF-β1/miR-21-5p signaling pathway in KCs might be a relevant approach to identify novel modulators of skin homeostasis with potential therapeutic applications in skin disorders. We found that silymarin (SM), a plant extract isolated from *Silybum marianum* (L.) Gaertn, regulated the functional activity of miR-21-5p through a SMAD-independent signaling pathway. We conducted an RNA-sequencing (RNA-seq) analysis combined with mechanistic studies to better delineate the effects of SM on KCs and reported unexpected biological roles of SM in KC differentiation and lipid synthesis. We further showed that SM might represent a promising approach for the treatment of psoriasis.

RESULTS

Design and validation of the screening strategy using the miR-ON RILES/21.5p T probe

To identify novel bioactive compounds potentially capable of modulating the TGF-β1/miR-21-5p signaling in KCs, we prepared a natural product library containing 37 crude extracts from medicinal plants (Table 1) and screened this library using the miR-ON RILES reporter system (Ezzine et al., 2013; Simion et al., 2021, 2020, 2017) (Figure 1a). The RILES system was placed under the control of the miR-21-5p by subcloning complementary blocks sequence to miR-21-5p in the 3′ untranslated region of the CymR transrepressor. The generated construct was called pRILES/21.5pT. When transfected in HaCaT cells, the pRILES/21.5pT probe will be either switched ON or OFF when the bioactive compounds delivered in cells will respectively modulate positively (upregulation) or negatively (downregulation) the expression of miR-21-5p (Figure 1). Consequently, the plant extracts enabled to modulate the TGF-β1/miR-21-5p signaling in cells will be identified by the emission of bioluminescence signals that can be captured using bioluminescence equipment. We evaluated the sensitivity and specificity of the pRILES/21.5pT probe by monitoring the endogenous expression of miR-21-5p in HaCaT cells in response to TGF-β1. Results from RT-qPCR studies indicated that maximal induction of miR-21-5p was reached when HaCaT cells were treated for 24 hours

Table 1. Plant Extract Library

Plant extract n°	Scientific Name
1	*Achillea millefolium* (L.)
2	*Alchemilla vulgaris* (L.)
3	*Arctium lappa* (L.)
4	*Arnica chamassonis*
5	*Artemisia annua* (L.)
6	*Artemisia vulgaris*
7	*Bacopa monnieri*
8	*Calendula officinalis*
9	*Centaurea cyanus*
10	*Centella asiatica* (L.)
11	*Cichorium intybus* (L.)
12	*Coleus blumei*
13	*Coleus forskohlii*
14	*Cyperus esculentus*
15	*Eclipta alba*
16	*Echinacea angustifolia*
17	*Echinacea purpurea* (L.) Moench
18	*Gentiana lutea* (L.)
19	*Iris pseudacorus* (L.)
20	*Lamium album*
21	*Lotus corniculatus*
22	*Ludwigia grandiflorum*
23	*Luronium natans* (L.) Raf
24	*Meconopsis betonicifolia*
25	*Melissa officinalis* (L.)
26	*Mentha piperita* (L.)
27	*Molinia caerulea* (L.)
28	*Physalis alkekengi*
29	*Prunus cesarus*
30	*Rosa*
31	*Salvia officinalis* (L.)
32	*Sylibum marianum* (L.) Gaertn
33	*Tephrosia purpurea*
34	*Trifolium pratense* (L.)
35	*Urtica dioica* (L.)
36	*Viola tricolor* (L.)
37	*Withania somnifera* (L.)

with 10 ng/ml of TGF-β1 (Figure 2a). Similar results were generated when the pRILES/21.5pT probe was transfected under the same experimental conditions (Figure 2b). In contrast, no change in luciferase expression was detected when the control pRILES plasmid, which did not contain a complementary block sequence to miR-21-5p, was used (Figure 2b) or when the pRILES/21.5pT probe was transfected in cells in the presence of miR-negative control or irrelevant miRs mimics as miR-206, miR-122, or miR-486 (Figure 2c). These results confirm (Ezzine et al., 2013; Simion et al., 2021, 2020) the specificity and sensitivity of our miR-ON RILES monitoring system and show that unlike the RT-qPCR detection system, the pRILES/21.5pT probe is a simple and fast execution system essential for the purpose of this study (e.g., cell-based miR screening assay).

Identification of *S. marianum* (L.) Gaertn as a potent modulator of the miR-21-5p in HaCaT cells treated with TGF-β1

Before the screening, we evaluated the relative toxicity of the 37 crude plant extracts to HaCaT cells. The *Whitania somnifera* (L.) crude extract was excluded from consideration owing to its toxicity at low concentration (e.g., 31 μg/ml, 36% toxicity ± 0.2%, data not shown). The screening procedure was conducted in a 96-well plate format in which HaCaT cells monolayers were first transfected with either the pRILES/21.5pT or pRILES control plasmid and then treated with TGF-β1 in the presence of serial dilutions of plant extracts (Figure 1). The purpose of including the pRILES control plasmid as well as a dose–response study in the screening procedure was to maximize our chances of identifying specific modulators of miR-21-5p expression while reducing the proportion of false-positive modulators that might regulate the expression of the luciferase reporter gene independently to the TGF-β1/miR-21-5p pathway. Results of this primary screening strategy led us to identify 3 of the 36 plant extracts that modulate the activity of luciferase by >1.5-fold in HaCaT cells treated with TGF-β1 compared with that in cells treated with TGF-β1 alone (Figure 1b). The *S. marianum* (L.) Gaertn, *Centella asiatica* (L.), and *Molinea caerulea* (L.) Moench extracts were identified as such (Figure 1b). To exclude the possibility that the increase in luciferase activity reflected an increase in cell proliferation, a second bioluminescent assay was performed in a 24-well plate format to normalize bioluminescence signals emitted from cells to protein content. As shown in Figure 1c, the three putative hits identified in the primary screening were confirmed for their specific induction of the luciferase reporter gene expression. The *S. marianum* (L.) Gaertn extract was identified as the most reactive plant extract. Indeed, when used as low as 15 μg/ml, this plant extract was sufficient to induce a significant change in the expression of the luciferase reporter gene, whereas 4-fold and 8-fold higher concentrations of plant extracts were required for *M. caerulea* (L.) Moench and *C. asiatica* (L.), respectively (Figure 1c).

The biological properties of *S. marianum* (L.) Gaertn. are attributed to SM, a mixture of eight major compounds, including seven flavonolignans (silibinin A, silibinin B, isosilibinin A, isosilybinin B, silychristin, isosilychristin, and silidianin) and one flavonoid (taxifolin). Silibinin, a complex of silibinin A and silibinin B in an approximately equimolar ratio, is the major bioactive constituent of SM (Kroll et al., 2007). Thus, we investigated whether the effect of our *S. marianum* (L.) Gaertn crude extract on luciferase activity emitted from the pRILES/21.5pT probe was dependent on SM and more specifically on silibinin. Our results showed that SM but not silibinin induced a similar dose-dependent increase of the luciferase activity in HaCaT cells compared with the *S. marianum* (L.) Gaertn extract (Figure 1d). Interestingly, neither *S. marianum* (L.) Gaertn extract nor SM modulated the expression of the luciferase reporter gene in the absence of TGF-β1 (data not shown). This result highlights the potential of this plant extract to regulate the expression of miR-21-5p only in response to an external stimulus.

Induction of miR-21-5p by SM in HaCaT cells treated with TGF-β1 involves a SMAD-independent signaling pathway

First, we validated that the effect of SM on RILES read out was miR-21-5p dependent. As shown in Figure 3a, the induction of the luciferase reporter gene was almost totally abolished when both TGF-β1 and TGF-β1 plus SM-treated HaCaT cells

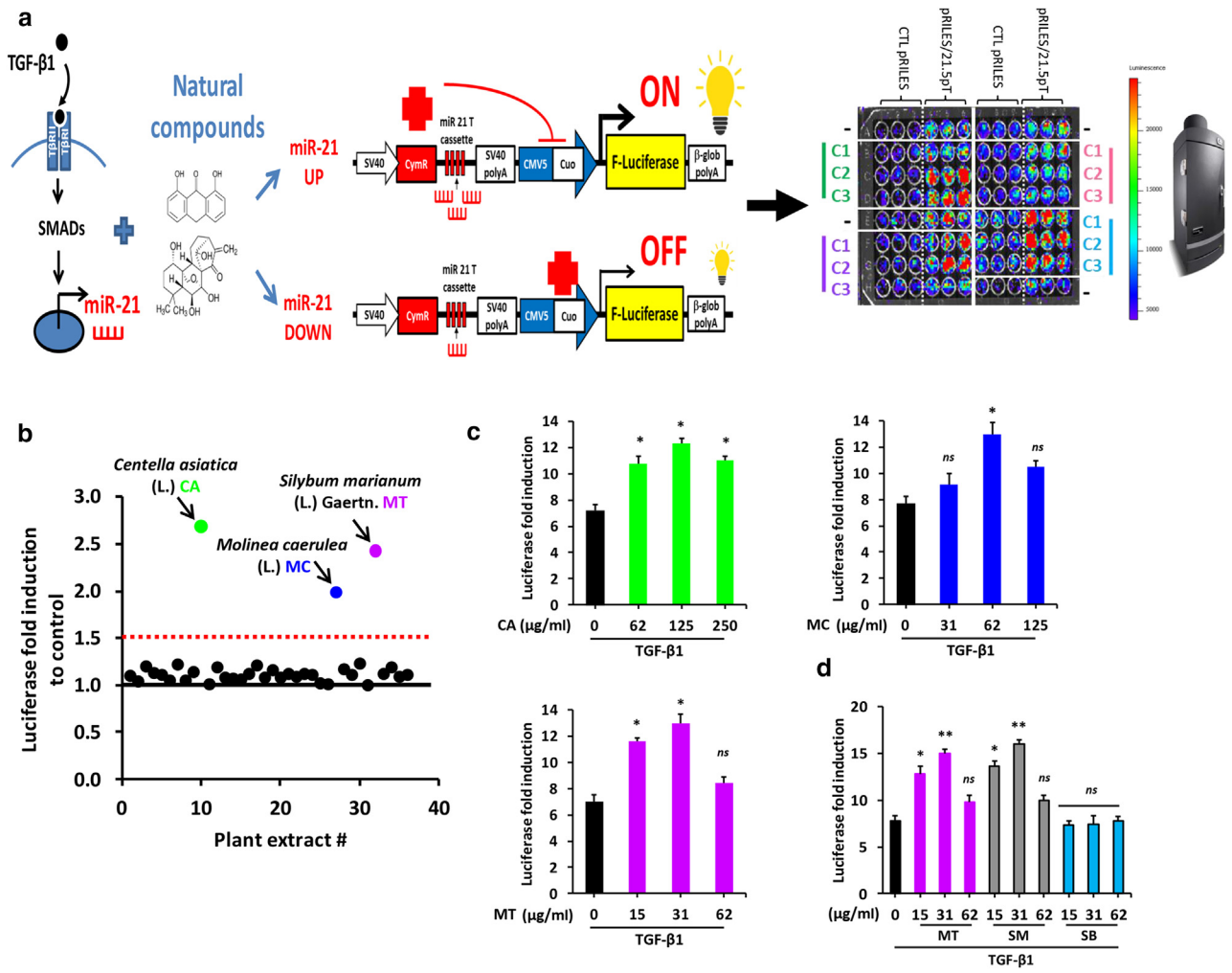

Figure 1. Identification of miR-21-5p modulators through plant extracts library screening. (**a**) Right panel: Schematic diagram of the screening procedure using the miR-ON RILES/21.5pT reporter system. The red cross corresponds to the CymR transrepressor protein. Left panel: representative 96-well plate generated after the screening of natural compounds using a bioluminescence imaging scanner. C1, C2, and C3 correspond to a serial dilution of a given compound. The green, purple, and blue colors represent three typical positive compounds, whereas the pink color represents a typical negative compound. HaCaT cells were transfected with either the pRILES/21.5pT or control pRILES plasmid and then treated with compounds prepared from a crude natural product extract library. Then, luciferase expression in cells was quantified and expressed as luciferase fold induction by dividing the relative bioluminescence values collected from cells transfected with the pRILES/21.5pT plasmid to bioluminescence values collected from cells transfected with the control, pRILES plasmid. Compounds enabled to generate in treated cells luciferase fold induction values different from luciferase fold induction values calculated in control cells treated with TGF-β1 alone, without any compound and referred to as −, were considered as positive hits. (**b**) Results of the primary screening of the natural products library. A total of 37 crude plant extracts were screened using this procedure. Green, blue, and purple dots represent the three miR-21-5p activators identified (hit rate of 8.3%). (**c, d**) Hits confirmation. The same procedure was used as in **a** but with cells grown in a 24-well plate and after normalization of bioluminescence values to total protein contents in cell lysates. Data are presented as mean ± SEM. Results for **c** and **d** are representative of three independent experiments performed in triplicate. Two-tailed unpaired *t*-test was used to test for significance between TGF-β1–treated cells with crude plant extracts and TGF-β1–treated cells alone. $*P < 0.05$ and $**P < 0.01$. CA, *Centella asiatica* (L.); MC, *Molinea caerulea* (L.); MT, *Silybum marianum* (L.) Gaertn; ns, not significant; SB, silibinin; SM, silymarin.

were transfected with miR-21-5p oligonucleotides inhibitors, attesting to the specificity of the induction. We next attempted to elucidate the mechanism responsible for the upregulation of miR-21-5p by SM in TGF-β1–treated HaCaT cells. We anticipated that it might be a direct consequence of the overactivation of the canonical TGF-β1 signaling pathway (Aashaq et al., 2022; Derynck and Zhang, 2003; Massagué, 1998). To test this hypothesis, we evaluated several functional aspects of the TGF-β1/SMAD signaling pathway. In contrast to what was expected, SM did not activate but rather inhibited the TGF-β1/SMAD signaling pathway. Significant downregulation of both SMAD2 (84% reduction) and SMAD3 (45% reduction) protein levels as well as the phosphorylated form of SMAD2 (30% reduction) were found in HaCaT cells treated with TGF-β1 plus SM used at the concentration of 62 μg/ml compared with that in cells treated with TGF-β1 alone (Figure 3b). We also found that SM inhibited the TGF-β1–induced epithelial–mesenchymal transition of HaCaT cells (Xu et al., 2009). Significant reduction of mesenchymal markers as fibronectin (84% reduction) and metalloproteinase-3 (76% reduction) and upregulation of the epithelial marker E-cadherin (39% increase) were detected in cells treated with TGF-β1 plus SM compared with that in cell treated with TGF-β1 alone (Figure 3c). Of note, the same pattern of downregulation of epithelial–mesenchymal transition markers induced by TGF-

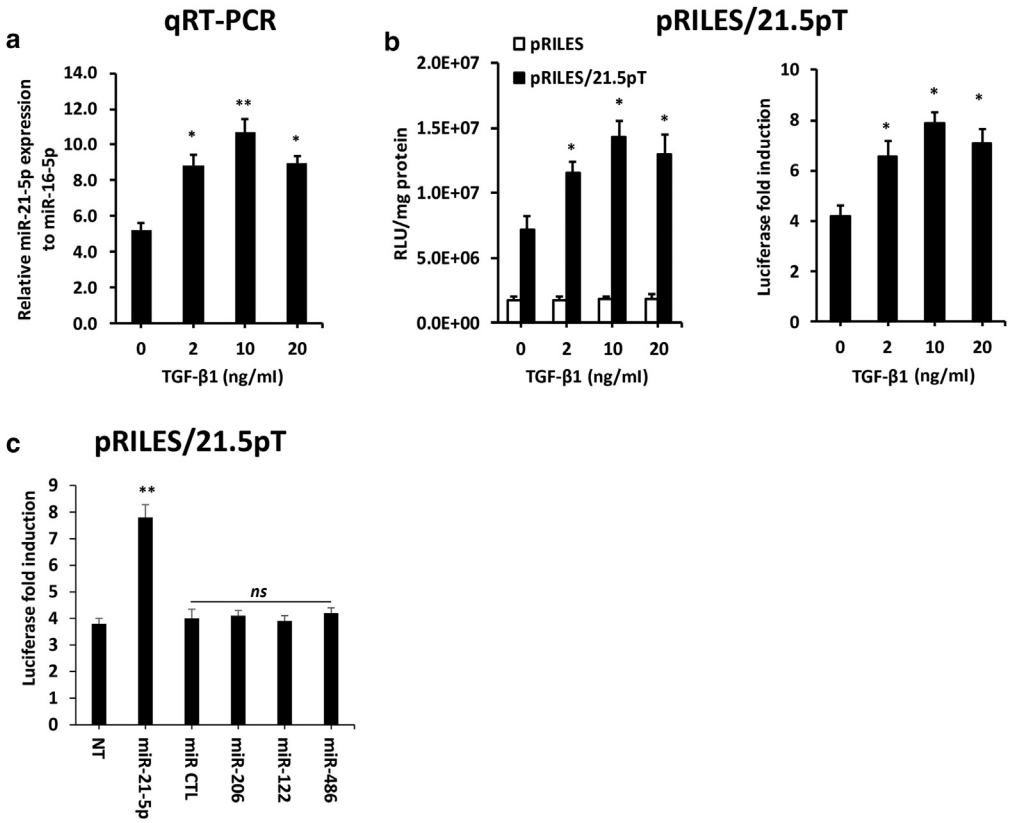

Figure 2. Validation of the pRILES/21.5pT sensitivity and specificity in keratinocytes. (**a**) HaCaT cells were treated with indicated concentrations of TGF-β1 for 24 h before quantifying the relative expression of miR-21-5p to miR-16-5p levels by RT-qPCR. (**b**) HaCaT cells were transfected with the control pRILES or pRILES/21.5pT plasmid and then treated with indicated concentrations of TGF-β1 for 24 h before quantifying the relative luciferase expression levels in cells using a luminometer. Data are presented as RLUs normalized to the total amount of proteins (mg) and expressed as luciferase fold induction relative to control cells transfected with the pRILES. (**c**) HaCaT cells were cotransfected with the control pRILES or pRILES/21.5pT plasmid in the presence of negative CTL, miR-21-5p, or irrelevant miRs (miR-206, -122, -486) mimics). Forty-eight hours after transfection, luciferase expression in cells was quantified and expressed as luciferase fold induction relative to control cells transfected with the pRILES. Data are presented as mean ± SEM and are representative of three independent experiments performed in triplicate. Two-tailed unpaired *t*-test was used to test for significance between TGF-β1– or synthetic miRNA–treated cells and control, not treated cells. $*P < 0.05$. CTL, control; h, hour; ns, not significant; RLU, relative light unit.

β1 treatment was also detected in primary human epidermal KCs treated with SM (e.g., normal human epidermal KC cells, data not shown). This correlated well with the drastic inhibition of the migratory behavior of HaCaT cells treated with TGF-β1 in a wound-healing scratch assay. As shown in Figure 3c, whereas complete wound closure was detected at 32 hours in wells treated with TGF-β1, the addition of SM totally abrogated this event. Taken together, these data indicate that SM mediated the induction of miR-21-5p in KCs in a SMAD-independent manner.

SM facilitates incorporation of the miR-21-5p into RNA-induced silencing complex

To gain further insight into the molecular mechanism where SM regulates miR-21-5p in HaCaT cells in response to TGF-β1, we quantified the expression levels of pri-miR-21, pre-miR-21, and mature miR-21-5p in cells by RT-qPCR. A significant increase in pri-miR-21 (∼9-fold), pre-miR-21 (∼5-fold), and mature miR-21-5p (∼2-fold) was detected in cells treated with TGF-β1 compared with that in non-treated control cells (Figure 4a). In contrast, no further changes or overexpression of miR-21-5p was detected in HaCaT cells treated with TGF-β1 plus SM (Figure 4a). The same was observed when experiments were performed in normal human epidermal KC cells. Transfection of the pRILES/21.5pT in these cells treated with TGF-β1 plus SM (31 μg/ml) switched-ON the RILES, whereas no statistically significant difference in terms of relative expression levels of the transcriptional forms of miR-21-5p was detected by RT-qPCR (data not shown). We therefore hypothesized that the induction of miR-21-5p in these cells would be more closely related to a greater loading of mature miR-21-5p into the RNA-induced silencing complex (RISC). To validate this point, we performed an RNA-binding protein immunoprecipitation assay using a specific anti-AGO2 antibody and quantified the amount of captured miR-21-5p by RT-qPCR. As shown in Figure 4b, the relative amount of miR-21-5p associated with AGO2-containing RISC was 1.9-fold higher in cells treated with TGF-β1 plus SM than in cells treated with TGF-β1 alone. This enrichment was not the result of overexpression of the *AGO2* gene in HaCaT cells because no changes in AGO2 protein levels were found in all samples analyzed (Figure 4c). To evaluate the functional impact of miR-21-5p enrichment into the RISC complex, we monitored the expression of some known transcriptional targets of miR-21-5p (Wang et al., 2020, 2012, 2009; Yang et al., 2014, 2011). As shown in Figure 4d, among the four tested transcriptional targets (IGFBP3, PDCD4, CDC25A, and TIMP3),

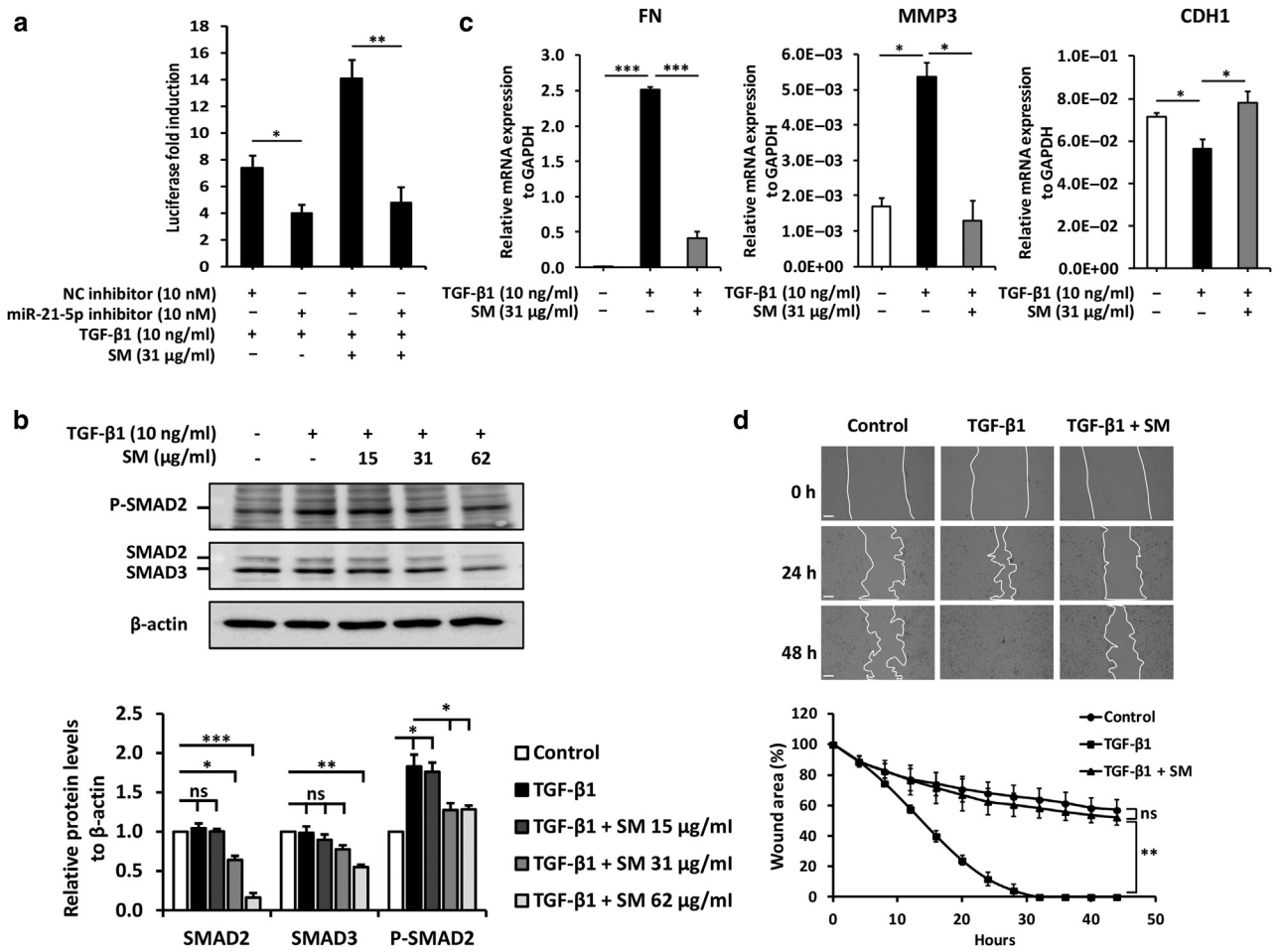

Figure 3. SM positively regulates miR-21-5p through a SMAD-independent signaling pathway in keratinocytes. (**a**) Quantitative bioluminescence values were detected in indicated HaCaT cell groups and expressed as luciferase fold induction relative to control cells transfected with the control pRILES. (**b**) Western blot analysis of SMAD2, SMAD3, and P-SMAD2 protein levels in total cell lysates from HaCaT cells treated with 10 ng/ml TGF-β1 in the presence or absence of indicated concentrations of SM for 1 h. β-Actin was used as a loading control. Band intensities were quantitatively analyzed using the ImageJ software. Bar graph data represent the ratio of protein of interest/β-actin. (**c**) RT-qPCR quantification of the relative expression of FN, MMP3, and CDH1 to GAPDH levels in HaCaT cells treated with 10 ng/ml TGF-β1 in the presence or absence of indicated concentrations of SM for 24 h. Untreated cells were used as the negative control. (**d**) In vitro scratch assay assessing the migration rate of HaCaT cells treated with 10 ng/ml TGF-β1 in the presence or absence of SM (31 μg/ml) for 48 h. Untreated cells were used as the negative control. The wound closure area was calculated using Zen 2.3 SP1 (Carl Zeiss, White Plains, NY). Data are presented as mean ± SEM and are representative of three independent experiments performed in triplicate. ANOVA test was applied to test for significance between the different groups in **a**, **b,** and **c.** Repeated measures ANOVA tests were used for **d**. $*P < 0.05$, $**P < 0.01$, and $***P < 0.001$. FN, fibronectin; h, hour; MMP3, metalloproteinase-3; ns, not significant; P-SMAD2, phosphorylated SMAD2; SM, silymarin.

three (IGFBP3, PDCD4, and CDC25A) were found statistically more downregulated in cells treated with TGF-β1 plus SM than in cells treated with TGF-β1 alone. Collectively, these data indicate that SM regulates the functional activity of miR-21-5p rather than its transcriptional expression and processing by Drosha and Dicer (Chendrimada et al., 2005; Denli et al., 2004; Lau et al., 2012; Lee et al., 2003; Yoshida et al., 2021).

SM causes global changes in the transcriptome of KCs

To more precisely define the impact of SM on the whole transcriptome of KCs, we conducted an RNA-seq analysis using total RNA fractions isolated from HaCaT cells treated with TGF-β1 plus SM versus those treated with TGF-β1 alone. A total of 605 differentially expressed genes (DEGs) were identified according to cutoff values of $\log_2$ fold change ≥ 1 and adjusted $P < 0.01$. A majority (434 of 605, 71%) were found downregulated (Figure 5a). Heatmap visualization indicated that the amplitude of gene expression was moderate with an average $\log_2$ fold change = 1.5. However, some DEGs achieved really high levels of regulation, as shown in Figure 5b. To further identify the biological functions enriched among the DEGs, a Gene Ontology and Kyoto Encyclopedia of Genes and Genomes bioinformatics analysis was performed. These analyses revealed that the most enriched biological processes from the downregulated DEGs were related to cell cycle processes including mitotic sister chromatid segregation, mitotic nuclear division, and chromosome segregation as well as to KC differentiation: cornification, epidermal cell differentiation, and keratinization. In contrast, the most enriched biological processes from the upregulated DEGs were related to lipid metabolism,

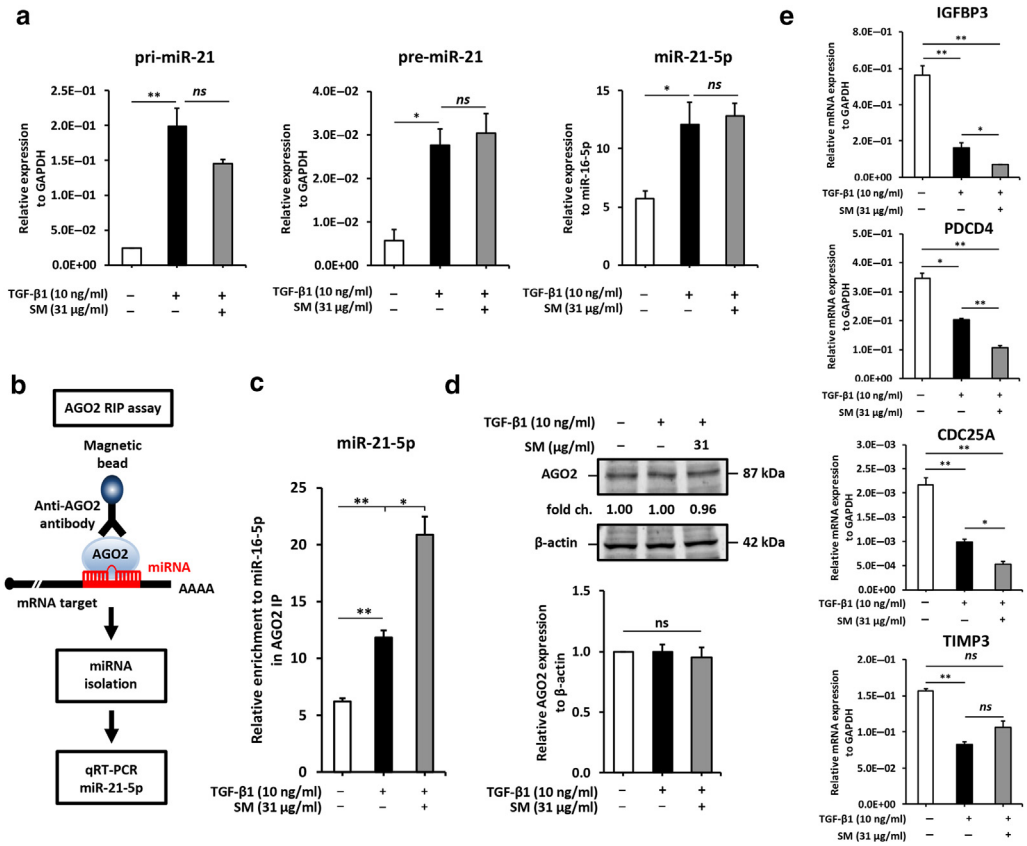

Figure 4. SM enhances miR-21-5p activity by promoting the loading of miR-21-5p into RISC. HaCaT cells were treated with 10 ng/ml TGF-β1 in the presence or absence of SM (31 µg/ml) for 24 h. Untreated cells were used as the negative control. (**a**) RT-qPCR quantification of relative pri-miR-21, pre-miR-21, and miR-21-5p levels. (**b**) Schematic diagram of AGO2-specific RIP assay. (**c**) Relative enrichment of miR-21-5p in the AGO2 IP complex detected by RT-qPCR. (**d**) Western blot analysis of AGO2 protein levels in total cell lysates from HaCaT cells. β-Actin was used as a loading control. Band intensities were quantitatively analyzed using the ImageJ software. Bar graph data represents the ratio of AGO2/GAPDH. (**e**) RT-qPCR quantification of the relative expression of IGFBP3, PDCD4, CDC25A, and TIMP3 to GAPDH levels in HaCaT cells. Data are presented as mean ± SEM and are representative of three independent experiments performed in triplicate. ANOVA test was applied to test for significance between the different groups. $*P < 0.05$ and $**P < 0.01$. h, hour; MMP3, matrix metalloproteinase 3; ns, not significant; RIP, RNA immunoprecipitation; RISC, RNA-induced silencing complex; SM, silymarin.

including coenzyme metabolic process, sterol metabolic process, and cholesterol biosynthetic process (Figure 5). The Gene Set Enrichment Analysis confirmed these results (Figure 5d). The top 15 downregulated and upregulated DEGs associated to these biological processes are listed in Figure 6.

SM regulates KC differentiation, proliferation, and lipid synthesis

Because the roles of SM in KC differentiation, proliferation, and lipid synthesis have not been reported before, we focused our next experiments on deciphering the molecular mechanisms underlying these biological processes.

We first investigated the biological effects of SM on the differentiation program of KCs. We evaluated the expression of differentiation markers in KCs induced to differentiate by TGF-β1 (Buschke et al., 2011; Kahata et al., 2018; Massagué, 2012; Matsumoto et al., 1990; Wang et al., 1999). In accordance with the RNA-seq data, treatment of HaCaT cells with TGF-β1 plus SM used at 62 µg/ml inhibited the expression of early (keratin [K]1, 81% inhibition and K10, 97% inhibition), intermediate (IVL, 96% inhibition), and late (FLG, 35% inhibition) differentiation markers induced by TGF-β1 (Figure 7a). We followed up this experiment by looking at the effect of SM on HaCaT cells induced to differentiate upon increase of calcium concentration in culture medium (Borowiec et al., 2013; Elsholz et al., 2014). HaCaT cells were cultured in low calcium (0.07 mM)–containing medium for several days to maintain cells in an undifferentiated status and then pushed to differentiate by subculturing the cells in a high calcium (HC) (1.8 mM)-containing medium for 9 consecutive days. As found in the model of differentiation of HaCaT cells induced by TGF-β1, the differentiation of cells induced by calcium switch was also inhibited by SM. Significant downregulation of *K10* (80% inhibition), *IVL* (50% inhibition), and *LOR* (47 % inhibition) gene expression was detected in cells treated with 62 µg/ml of SM compared with that in untreated cells cultured in HC-containing medium (Figure 7b,c). A similar reduction in *K10*, *IVL*, and *LOR* mRNA levels was also detected by RT-qPCR in normal human epidermal KC cells induced to differentiate by calcium switch (data not shown). Interestingly, the inhibitory effect of SM was comparable with that of the well-known negative regulator of KC differentiation, all-trans retinoic acid used at 1 µM (Figure 7c). Because NOTCH signaling promotes the commitment of KCs to differentiation (Flora and Ezhkova, 2020; Nguyen et al., 2006),

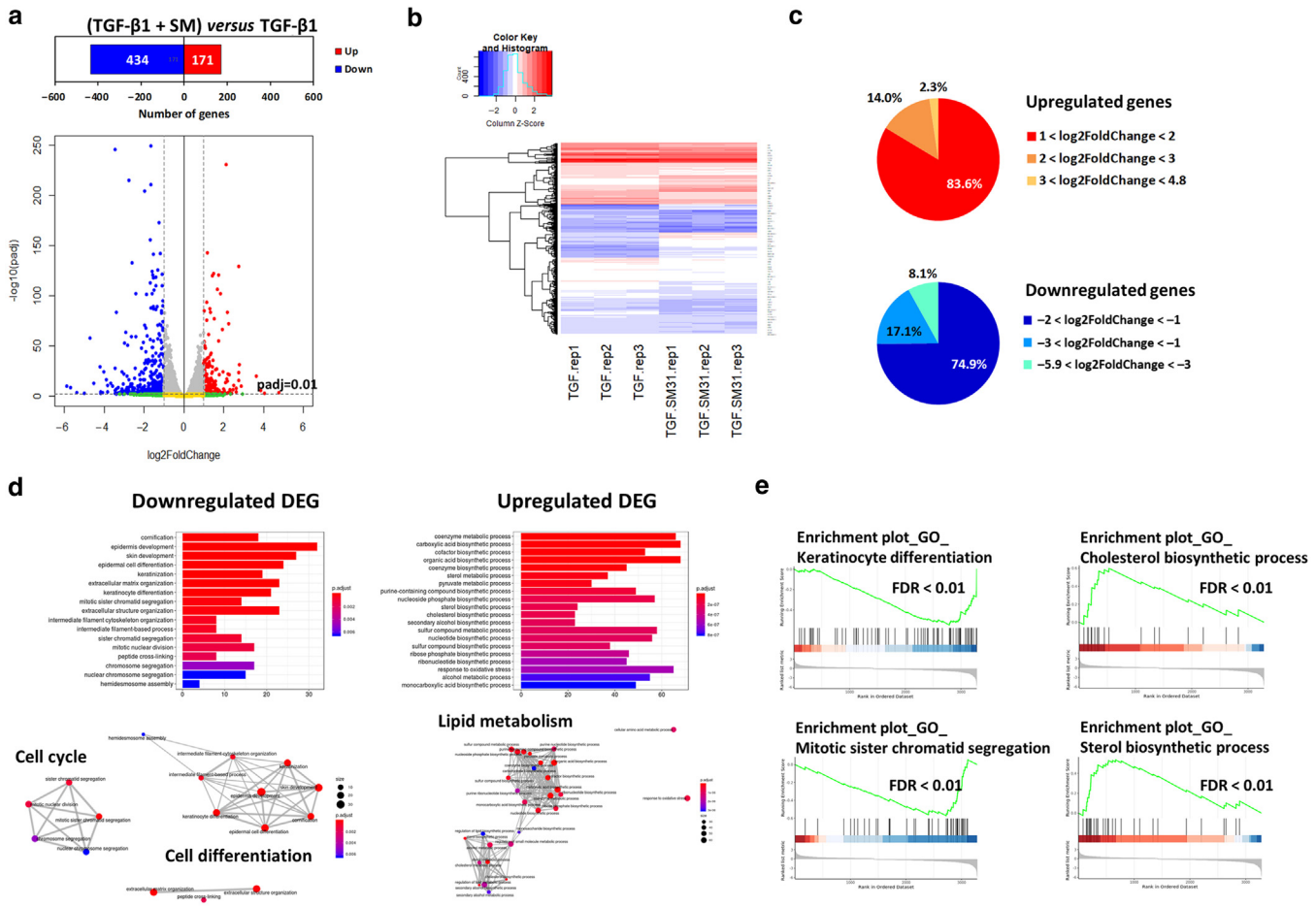

Figure 5. SM induces global changes in the keratinocyte transcriptome. (**a**) Volcano plot displaying differentially expressed genes between HaCaT cells treated with 10 ng/ml TGF-β1 in the presence of SM (31 μg/ml) and HaCaT cells treated with 10 ng/ml TGF-β1 alone for 24 h. Scattered points represent genes. The x-axis corresponds to the $\log_2$ fold change, and the y-axis corresponds to the $-\log_{10}$ *P*adj. Blue dots are genes significantly downregulated (*P*adj < 0.01, $\log_2$ fold change < −1), whereas red dots are genes significantly upregulated (*P*adj < 0.01, $\log_2$ fold change > 1). (**b**) Heatmap of the upregulated (n = 171) and downregulated (n = 434) differentially expressed genes between the two conditions (*P*adj < 0.01, −1 > $\log_2$ fold change > 1). (**c**) Venn diagrams displaying the percentage of upregulated and downregulated differentially expressed genes depending on the change of their expression. (**d**) Functional analysis of genes altered by SM. The results of the GO enrichment analysis are represented as a bar plot and a network plot. The network plot depicts the linkage of enriched GO terms. Left panel: The top 15 most enriched GO biological processes terms of the downregulated differentially expressed genes. Right panel: The top 20 most enriched GO biological processes terms of the upregulated differentially expressed genes. The color coding (red, purple, blue) represents the adjusted *P*-value, whereas the bar height/dot size represents the number of genes involved in each GO term. (**e**) GSEA. Genes were ranked according to their expression from the downregulated at the left to upregulated at the right. The y-axis indicates enrichment scores (top) and ranked list metric (bottom). X-axis bars represent individual genes for the indicated gene sets. DEG, differentially expressed gene; GO, Gene Ontology; GSEA, Gene Set Enrichment Analysis; h, hour; *P*adj, adjusted *P*-value.

we then looked at the expression level of NOTCH isoforms in HaCaT cells induced to differentiate by calcium switch. Among the three Notch isoforms evaluated (i.e., NOTCH1, 2, and 3), NOTCH3 expression was found significantly downregulated by SM and in a dose-dependent manner (Figure 7e). Time course analysis revealed that SM downregulated NOTCH3 protein levels as early as 15 minutes after calcium-induced differentiation of HaCaT cells (Figure 7). These results indicate that SM affects the KC differentiation program in a NOTCH3-dependent manner and at early time points.

Because KC differentiation is accompanied by a decrease in their proliferation rate (McMullan et al., 2003; Missero et al., 1995; Nguyen et al., 2006; Truong et al., 2006), we examined the effect of SM on the cell cycle of HaCaT cells cultured in HC-containing medium. Results in Figure 8a revealed that treatment of cells with SM for 24 hours led to a gradual accumulation of cells in the G0/G1 phase according to the dose of SM used that correlated with a gradual decrease of the percentage of cells in the G2/M phase. The reduction in the proliferation rate of HaCaT cells by SM was not the result of the induction of apoptosis in these cells. Annexin V/PI staining of these cells did not lead to the detection of apoptotic and necrotic cells but rather revealed a slight increase in the percentage of viable cells (Figure 8b). This indicates that SM exerts an inhibitory effect on HaCaT cell growth without inducing cell death.

Then, we seek to identify the processes by which SM might induce the expression of lipogenic genes *ACLY*, *ACSS2*, and *FASN* highlighted by the bioinformatics analysis of our RNA-seq data. qRT-PCR analysis confirmed that treatment of

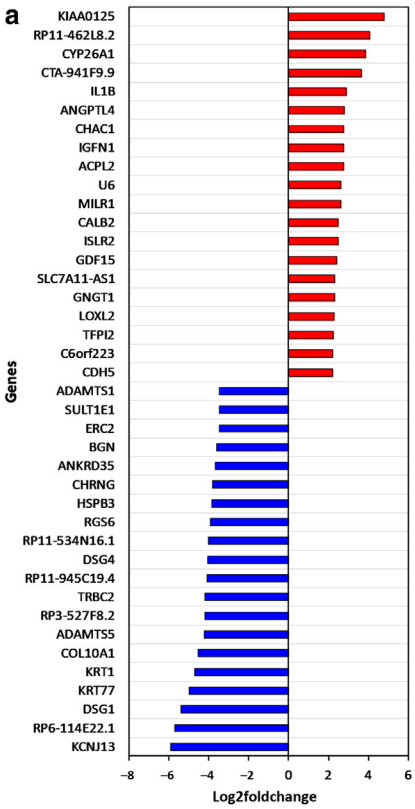

b

Upregulated DEG		
Lipid metabolism		
Gene name	Fold change	Padj
ACSS2	2.38	9.74E-13
FASN	2.38	3.30E-14
ACLY	2.00	4.64E-33
IDI1	1.97	8.49E-54
TM7SF2	1.92	2.43E-15
LIPE	1.89	2.50E-07
MSMO1	1.83	1.74E-46
INSIG1	1.80	2.20E-49
MVD	1.77	2.78E-04
DHCR7	1.77	1.85E-22
FDFT1	1.76	3.11E-39
G6PD	1.76	7.11E-19
ELOVL7	1.75	8.48E-06
STXBP1	1.68	5.61E-17
HMGCS1	1.68	5.43E-36

c

Downregulated DEG				
Keratinocyte differentiation			Cell division	
Gene name	Fold change	padj	Gene name	Fold change padj
K1	−26.23	2.59e-58	*HMCN1*	−6.29	1.71E-59
DSG4	−16.59	8.98e-250	*FAM64A*	−4.71	8.80E-10
FOXN1	−4.28	6.62E-07	*KIF20A*	−4.08	4.58E-54
SPRR1B	−3.93	2.60E-33	*TTC28*	−3.06	4.63E-49
SPRR1B	−3.93	2.60E-33	*GTSE1*	−2.92	5.55E-11
TXNIP	−3.20	8.96E-250	*MKI67*	−2.90	1.11E-88
IVL	−3.05	8.48E-125	*NCAPG*	−2.86	4.73E-09
TGM1	−2.97	1.76E-36	*KIF2C*	−2.78	9.27E-11
SPINK5	−2.83	6.34E-16	*KIF18B*	−2.56	7.31E-07
K16	−2.69	3.72E-36	*CENPE*	−2.45	6.81E-14
K4	−2.68	1.27E-35	*ASPM*	−2.37	3.79E-40
ID3	−2.50	2.06E-71	*NDC80*	−2.30	1.41E-03
K3	−2.24	2.74E-05	*BUB1B*	−2.29	1.34E-06
K14	−2.20	1.77E-83	*KIF14*	−2.27	4.64E-14
ABCA12	−2.08	4.64E-05	*KIF4B*	−2.13	7.29E-03

Figure 6. List of the top 20 upregulated and downregulated DEGs according to their log_2 fold change value. DEG, differentially expressed gene.

HaCaT cells with TGF-β1 plus SM significantly induced the expression of *ACLY*, *ACSS2*, and *FASN* mRNA compared with treatment with TGF-β1 alone (Figure 9a). To determine the signaling pathways responsible for the transcriptional activation of these lipogenic genes, we performed a Kyoto Encyclopedia of Genes and Genomes pathway enrichment analysis. A significant enrichment ($P < 0.05$) of upregulated DEGs in the peroxisome proliferator–activated receptor (PPAR) signaling pathway was found. The PPAR family comprises three subtypes (PPARα, PPARβ/δ, and PPARγ), which are expressed in human KCs (Rivier et al., 1998). Among the three subtypes, PPARγ is considered a major regulator of epidermal lipid metabolism (Mao-Qiang et al., 2004; Ramot et al., 2015; Schmuth et al., 2014). We therefore examined whether SM could activate PPARγ activity using a reporter luciferase gene construct containing PPARγ responsive elements (i.e., PPRE-Luc plasmid). As anticipated, HaCaT cells induced to differentiate by TGF-β1 exhibited an elevated PPARγ activity that was further increased in the presence of SM. A maximum of 1.6-fold increase in luciferase activity was detected when SM was used at the concentration of 31 μg/ml (Figure 9b). To determine whether a similar event could also occur in the model of calcium-induced KC differentiation, we looked at the gene expression of *ACLY*, *ACSS2*, and *FASN* in HaCaT cells grown in low calcium–containing medium and induced to differentiate in an HC-containing medium in the presence of SM. Results revealed, once again, that the expressions of *ACLY*, *ACSS2*, and *FASN* were significantly upregulated in HaCaT cells induced to differentiate by calcium switch when SM was added to the culture medium in a time- and dose-dependent manner. To validate that the changes in the expression of lipogenic genes led to lipid production in cells, monolayers of HaCaT cells treated with SM were stained with Oil Red O. A clear increase, in both number and size, of stained intracellular lipid droplets was observed in HaCaT cells cultured for 9 days in HC-containing medium in the presence of SM (Figure 9c). A similar induction of intracellular lipid droplets was detected in calcium chloride–differentiated normal human epidermal KC cells stained with Oil Red O after treatment with SM, which correlated with statistically significant induction of relative expression levels of lipogenic genes *ACLY*, *ACSS2*, and *FASN* (data not shown). Several reports indicate that AMP-activated protein kinase (AMPK) acts as a central regulator of energy homeostasis by decreasing the adenosine triphosphate–consuming anabolic processes, such as the synthesis of cholesterol and fatty acid (Herzig and Shaw, 2018). We therefore examined whether SM might regulate the activation of AMPK. Western blot analysis (Figure 9d) revealed that the treatment of HaCaT cells, grown in low calcium–containing medium, with SM in HC-containing medium resulted in a time-dependent decrease in AMPK phosphorylation (a maximum of 36.6% decrease was seen after 15 minutes of differentiation compared with that in the control cells) without affecting total AMPK levels. Next, we looked at the activity of SREBP-1c, known as a master lipogenic regulator whose activity is abrogated by the phosphorylation of AMPK (Hawley et al., 1996; Li et al., 2011b). We thus focused our attention to the consequences of inhibition of AMPK phosphorylation by SM on SREBP-1c

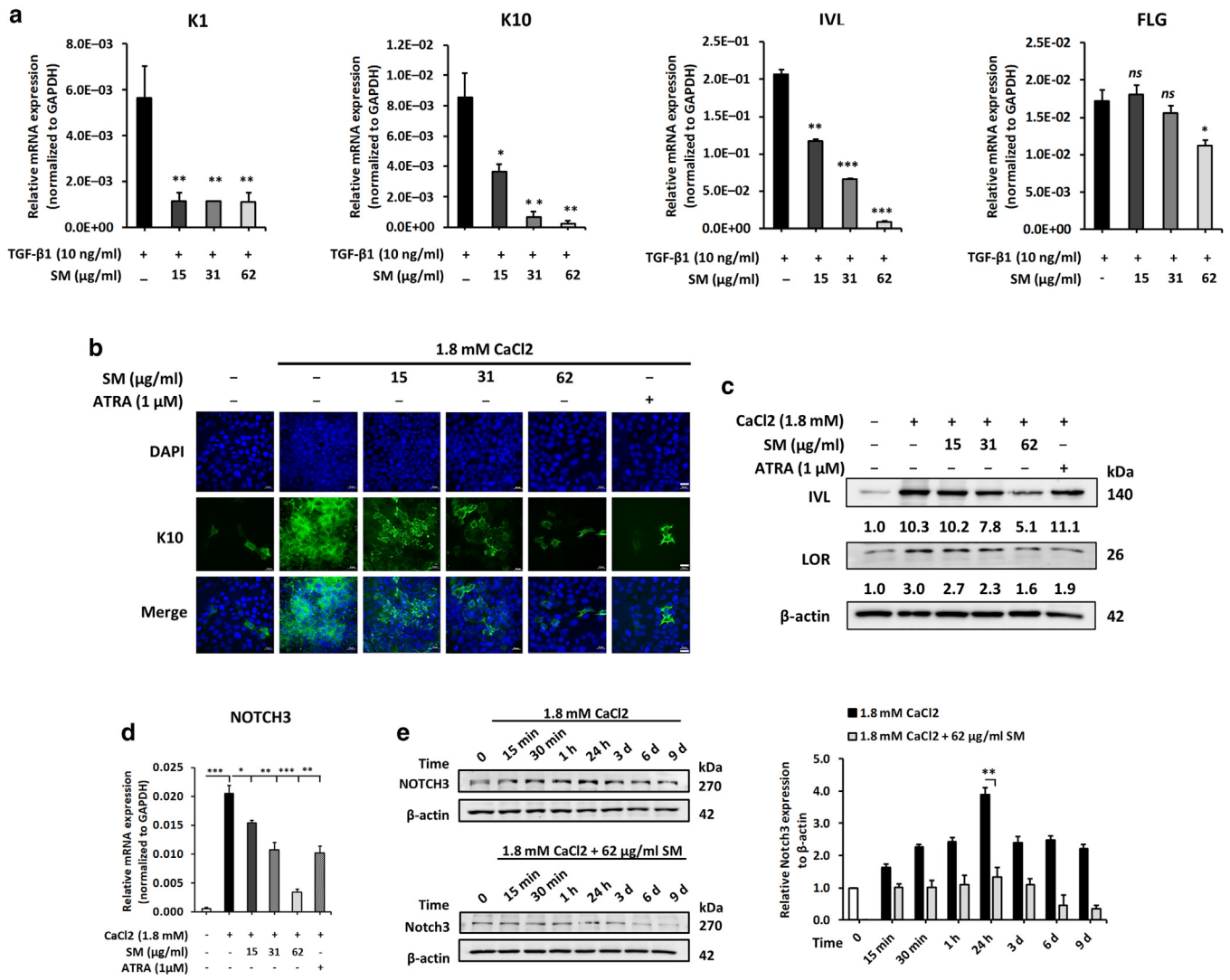

Figure 7. SM blocks the keratinocyte proliferation–differentiation switch through the inhibition of NOTCH3. (**a**) RT-qPCR quantification of relative expression of K1, K10, IVL, and FLG to GAPDH levels in HaCaT cells treated with 10 ng/ml TGF-β1 in the presence or absence of indicated concentrations of SM for 24 h. (**b–e**) HaCaT cells were maintained in low calcium (0.07 mM)–containing medium and then switched to high calcium (1.8 mM)–containing medium for 9 days in the presence or absence of indicated concentrations of SM. ATRA (1 μM) was used as a negative control. (**b**) Immunofluorescence staining of K10. Bar = 20 μM. (**c**) Western blot analysis of IVL and LOR protein levels. β-Actin was used as a protein loading control. Band intensities were quantitatively analyzed using the ImageJ software. (**d**) The relative gene expression of NOTCH3 to GAPDH was analyzed by RT-qPCR. (**e**) Western blot analysis showing the time course of NOTCH3 protein expression in HaCaT cells treated with SM (62 μg/ml). β-Actin was used as a loading control. Data are presented as mean ± SEM and are representative of three independent experiments performed in triplicate. Two-tailed unpaired *t*-test was applied for **a** to test for significance between TGF-β1–treated cells with SM and TGF-β1–treated cells alone. ANOVA test was used for **d** for multiple comparison between the different groups. Two-tailed unpaired *t*-test was applied for **e** to test for significance between CaCl2-treated cells with SM and CaCl2-treated cells alone at the 24 h time point, chosen arbitrarily. *$P < 0.05$, **$P < 0.01$, and **$P < 0.001$. ATRA, all-trans retinoid acid; CaCl2, calcium chloride; FDR, false discovery rate; GO, Gene Ontology; h, hour; IVL, involucrin; K, keratin; LOR, loricrin; ns, not significant; SM, silymarin.

processing in HaCaT cells. Contrary to expectations, whereas the mature form of SREBP-1c was seen in protein lysates of HaCaT cells induced to differentiate in HC-containing medium, treatment of cells with SM completely blocked SREBP-1c processing as early as 3 days after treatment (Figure 9e). These results indicate that SM regulates the lipid metabolism in HaCaT cells independently of AMPK/SREBP-1c signaling but at least through PPARγ signaling.

SM inhibits inflammation in KCs

Very few studies have assessed the anti-inflammatory properties of SM on KCs (Frankova et al., 2021), although it is considered to be relevant for the treatment of inflammatory skin diseases. We conducted this evaluation to further appreciate the roles of SM in skin biology. First, we investigated the protective role of SM on TNF-α–induced IL-6 production in HaCaT cells. As expected, results from ELISA assay showed that the stimulation of HaCaT cells with TNF-α for 24 hours led to a robust increase in the secreted amounts of IL-6 (65.19 ± 5.31 pg/ml) compared with that of the control, untreated cells (18.27 ± 1.12 pg/ml) (Figure 10a). Costimulation of TNF-α with SM significantly inhibited this process with a maximum of 3-fold decrease ($P < 0.01$) in IL-6 production (Figure 10a). The same inhibitory effect was

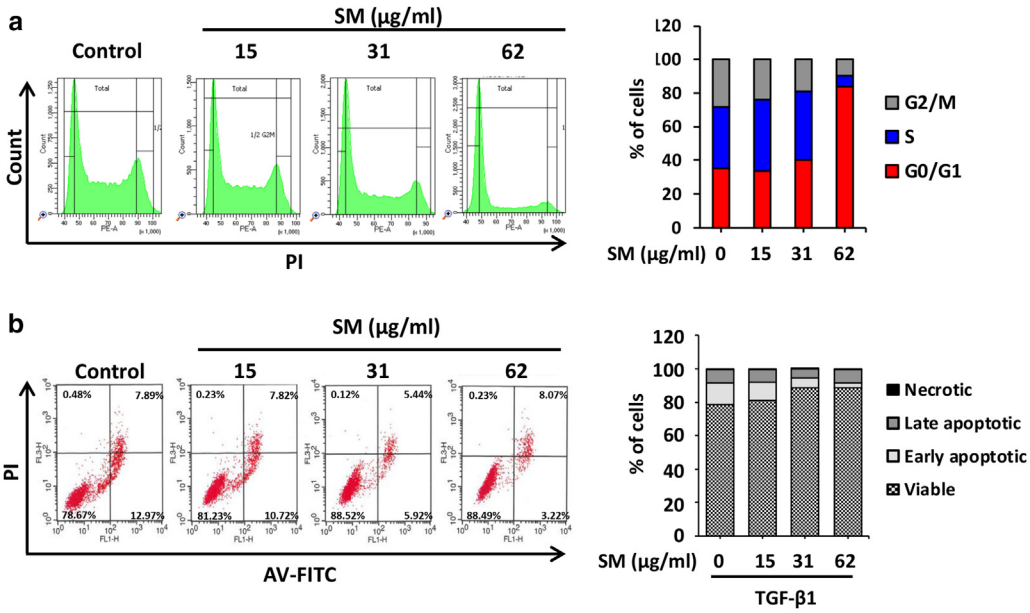

Figure 8. SM induces G0/G1 cell cycle arrest without inducing apoptotic cell death in keratinocytes. (**a**) HaCaT cells were treated with indicated concentrations of SM for 24 h before analyzing cell cycle distribution by flow cytometry. Untreated cells were used as the negative control. (**b**) HaCaT cells were treated with TGF-β1 in the presence or absence of indicated concentrations of SM for 24 h. The cells were collected and incubated with AV-FITC and PI for flow cytometry analysis. Numbers indicate the percentage of cells within the indicated gate. Results are representative of three independent experiments performed in triplicate. AV, annexin V; h, hour; *P*adj, adjusted *P*-value; PI, propidium iodide; SM, silymarin.

observed when cells were exposed to UVB irradiation to induce the expression of cyclooxygenase-2 (Wilgus et al., 2000). Indeed, pretreatment of HaCaT cells with SM before UVB irradiation suppressed almost totally the induction of cyclooxygenase-2 protein expression (Figure 10b). To gain insight into the molecular mechanisms regulating the anti-inflammatory responses of SM, HaCaT cells were transfected with a reporter luciferase gene construct containing NF-κB responsive elements (i.e., NF-κB-Luc plasmid) and then treated with SM and IL-22, another potent proinflammatory cytokine that activates the NF-κB signaling pathway (Abdallah et al., 2021). As shown in Figure 10c, the treatment of HaCaT cells with SM and IL-22 repressed almost totally the induction of NF-κB–driven luciferase activity. Altogether, these data indicate that SM is a potent inhibitor of inflammatory response by interfering with the NF-κB signaling pathway in HaCaT cells.

Topical SM treatment ameliorates imiquimod-induced psoriasis-like skin inflammation in mice

On the basis of the biological properties that we assigned to SM in this study, we anticipated that this plant extract could be used to treat inflammatory skin diseases. We focused on psoriasis because this common chronic inflammatory skin disease is characterized by abnormal differentiation and hyperproliferation of epidermal KCs (Griffiths and Barker, 2007). We validated this hypothesis using the imiquimod (IMQ)-induced psoriasis mouse model (van der Fits et al., 2009). Three groups of mice were topically treated with either acetone (control group), 5% IMQ cream (IMQ group), or SM before 5% IMQ cream (IMQ + SM group) for 6 consecutive days on their shaved back skin (Figure 11). As expected, on day 4, the IMQ-treated mice exhibited erythematous, thickened, and scaly back skin compared with the control mice. Remarkably, pretreatment with SM considerably attenuated these phenotypical changes as attested by a 92% reduction in the cumulative PASI (Figure 11c). Histological analysis of back skin tissue sections showed that topical SM pretreatment greatly reduced acanthosis, hyperkeratosis, parakeratosis, and dermal infiltrating cells compared with that in IMQ-treated skin (Figure 11d). Moreover, SM-pretreated mice exhibited a 1.4-fold decrease ($P < 0.05$) in the number of Ki-67–positive KCs that was associated with a statistically significant reduction in epidermal thickness (Figure 11e).

SM reduces inflammation and restores the differentiation program of epidermal KCs in IMQ-induced psoriasis-like skin lesions in mice

To further strengthen our findings, we next quantified the expression levels of proinflammatory genes in skin samples of each group of mice. Consistent with the histological changes, SM pretreatment before IMQ application significantly downregulated the expression of psoriasis-associated inflammatory cytokines (IL-23A and IL-22), chemokines (CCL20 and CXCL1), and antimicrobial peptides (S100A8 and S100A9), which were found aberrantly expressed in the IMQ-treated group (Figure 12). These results indicate that SM is capable to suppress inflammation in IMQ-induced psoriasis-like skin lesions in mice. Because previous studies have reported that terminal differentiation of KCs is significantly impaired in psoriatic skin lesions (Lowes et al., 2007; Nestle et al., 2009), we looked at the expression levels of early and late differentiation KC markers in skin samples of mice. qRT-PCR analysis indicated that IMQ treatment significantly decreased the relative expression of *K10*, *Ivl*, and *Lor* by 5.3, 2.2, and 8.8-fold, respectively, compared with the expression in control mice (Figure 12). Remarkably, SM pretreatment

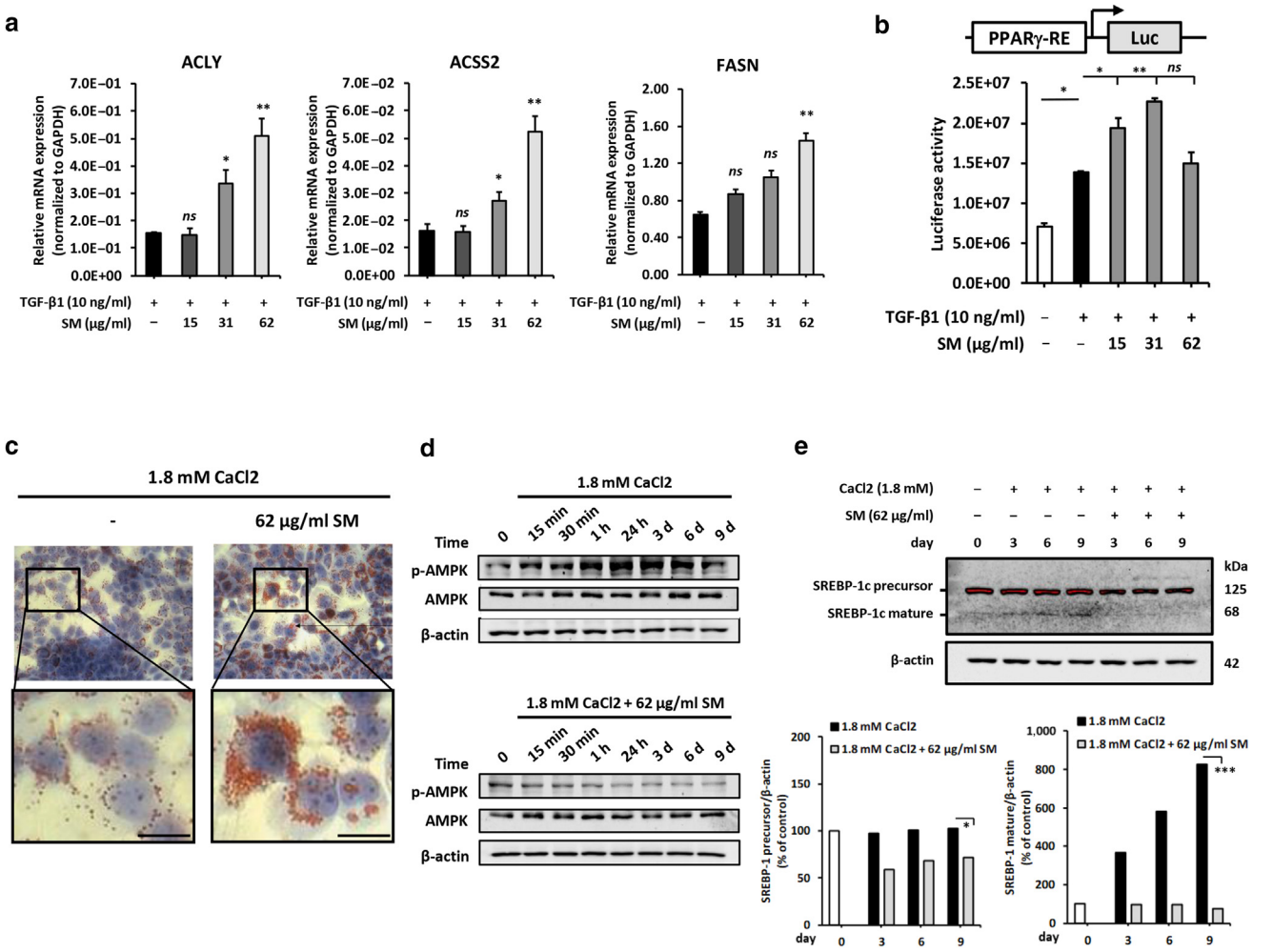

Figure 9. SM enhances lipid synthesis and accumulation in keratinocytes in an SREBP-1c–independent and PPAR-γ–dependent manner. (**a**) HaCaT cells were treated with TGF-β1 in the presence or absence of indicated concentrations of SM for 24 h before quantifying the relative expression levels of *ACLY*, *ACSS2*, and *FASN* by RT-qPCR. (**b**) HaCaT cells were transfected with a reporter construct carrying a PPRE-driven luciferase gene and then treated with 10 ng/ml TGF-β1 in the presence or absence of indicated concentrations of SM. Untreated cells were used as the negative control. Luciferase activity was measured 24 h later. (**c–e**) HaCaT cells were maintained in low calcium (0.07 mM)–containing medium and then switched to high calcium (1.8 mM)–containing medium for 9 days in the presence or absence of SM (62 μg/ml). At the end of the treatment, (**c**) lipid droplets in HaCaT cells were revealed by Oil Red O staining and examined using a microscope equipped with a digital camera. Square boxes are the zoomed images. Bar = 50 μm. (**d**) Time course analysis of total and p-AMPK protein levels in HaCaT cells by western blot. β-Actin was used as a loading control. (**e**) Western blot analysis of the precursor and mature forms of SREBP-1c. β-Actin was used as a loading control. Band intensities were analyzed using the ImageJ software. Bar graphs data represent the ratio of SREBP-1c precursor/β-actin and SREBP-1c mature/β-actin. Data are presented as mean ± SEM and are representative of three experiments performed in triplicate. Two-tailed unpaired *t*-test was applied for **a** to test for significance between TGF-β1–treated cells with SM and TGF-β1–treated cells alone. ANOVA test was used for **b** for multiple comparison between the different groups. Two-tailed unpaired *t*-test was applied for **e** to test for significance between CaCl2-treated cells with SM and CaCl2-treated cells alone at the 9-day time point, chosen arbitrarily. $*P < 0.05$ and $**P < 0.01$. AMPK, AMP-activated protein kinase; ATP, adenosine triphosphate; CaCl2, calcium chloride; h, hour; K, keratin; min, minute; ns, not significant; p-AMPK, phosphorylated AMP-activated protein kinase; PPAR-γ, peroxisome proliferator–activated receptor γ; PPRE, peroxisome proliferator response element; SM, silymarin.

before the application of IMQ was found sufficient to restore the gene expression pattern of these markers to expression levels similar to those in the control group of mice. These data show that SM corrects the differentiation program of KC in IMQ-induced psoriasis skin lesions in mice.

SM restores the expression of genes involved in lipid metabolism in IMQ-induced psoriasis-like skin lesions in mice

Increasing evidence has shown a close relationship between psoriasis and dyslipidemia (Chapkin et al., 1986; Ma et al., 2014; Nakajima et al., 2013). Studies have reported reduced expression of free fatty acids and ceramides content in the lesional skin of patients with psoriasis in comparison with expression in the skin samples of healthy controls (Chapkin et al., 1986; Nakajima et al., 2013). Nevertheless, the underlying molecular mechanisms remain unknown. Because we expected that SM pretreatment before IMQ would rescue dysregulated lipid metabolism in epidermal cells, we first evaluated the relevance of our hypothesis by looking at the expression of *ACSS2* and *FASN* in normal skin of healthy volunteers (n = 10) and in lesional skin of patients with psoriasis (n = 9). qRT-PCR analysis revealed significantly lower expression levels of these markers in lesional psoriatic samples than in normal skin (Figure 13a). Consequently, we next assessed the effect of SM on the gene expression of these markers in the IMQ-induced psoriasis mouse model. As for

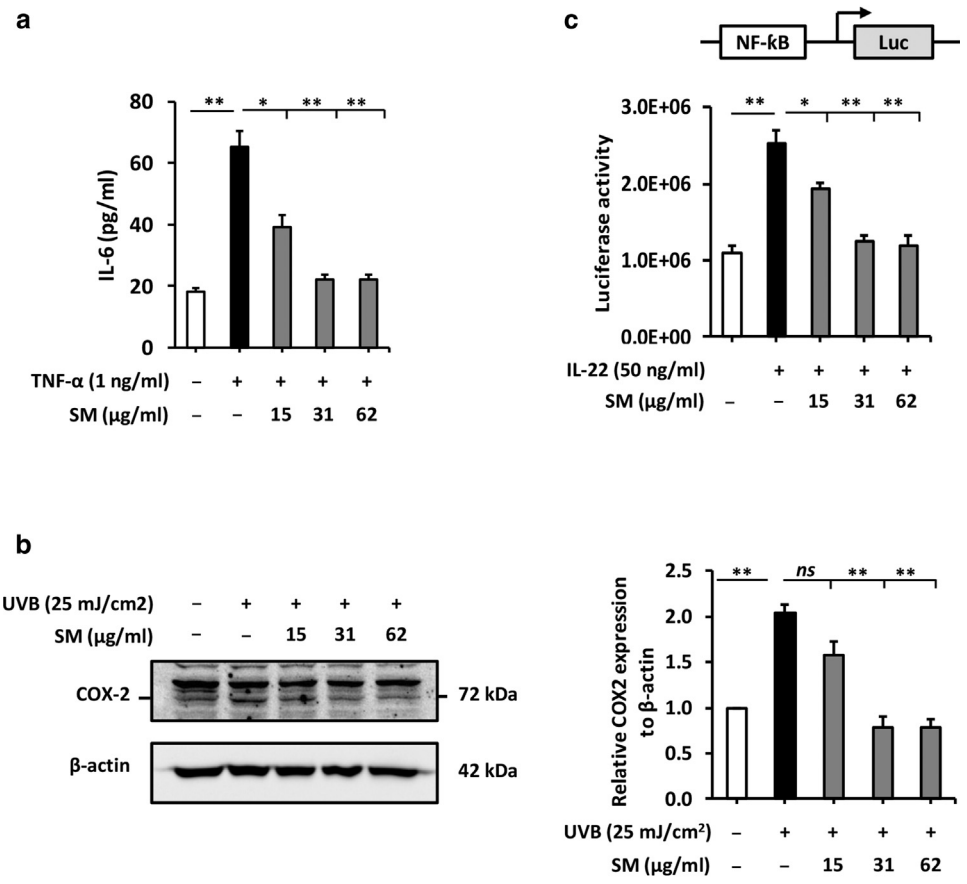

Figure 10. SM has anti-inflammatory activities in keratinocytes. (**a**) ELISA quantification of IL-6 production in HaCaT cells treated with TNF-α in the presence or absence of indicated concentrations of SM for 24 h. Untreated cells were used as the negative control. (**b**) Western blot analysis of COX2 expression in HaCaT cells pretreated with indicated concentrations of SM before irradiation to UVB. β-Actin was used as a loading control. (**c**) NF-κB luciferase reporter activity quantified in HaCaT cells transfected with NF-κB-Luc plasmid construct before treatment with IL-22 (50 ng/ml for 24 h) in the presence or absence of indicated concentrations of SM. Data are presented as mean ± SEM and are representative of three independent experiments performed in triplicate. ANOVA test was applied to test for significance between the different groups. $*P < 0.05$ and $**P < 0.01$. AV, annexin V; COX2, cycloxygenase-2; h, hour; ns, not significant; PI, propidium iodide; SM, silymarin.

the clinical samples, significant decreases in *Acss2* (3.3-fold) and *Fasn* (4.8-fold) expression was detected in IMQ-treated mice compared with that in control mice, together with significantly decreased expression of *Srebf1* (2.7-fold) and *Acly* (7.1-fold) (Figure 13b). Remarkably, pretreatment of mice with SM before IMQ restored normal expression patterns of these genes. Therefore, in addition to its antiproliferative, prodifferentiation, and anti-inflammatory effects, SM corrects as well the impaired lipid metabolism in IMQ-induced psoriatic skin lesions in mice.

Finally, we addressed the safety and possible adverse events of SM when applied topically on mouse skin. No major macroscopic or microscopic changes in the morphology of skin tissues of SM-treated mice were detected, although a noticeable change in the thickness of the epidermis could be observed (Figure 14a,b). Such an increase in the thickness of the epidermis can be explained by an increase in the proliferative state of KCs in the basal layer of the epidermis, as revealed by Ki-67 immunostaining of tissue sections of SM-treated mice (Figure 14c). As a consequence, the relative gene expression levels of differentiation markers *K10, Ivl,* and *Lor* were found statistically significantly upregulated in the SM-treated mice compared with that in the control, not treated mice (Figure 14d). Nevertheless, no inflammatory reactions were detected in these tissues because none of the six inflammatory markers quantified by RT-qPCR showed a statistically significant difference in terms of expression between SM-treated mice and control, not-treated mice (Figure 14e). Furthermore, no major change in the expression level of lipid markers was also observed. Among the four lipids markers quantified (*SREBF1*, *ACLY*, *ACSS2*, and *FASN*), only the *ACSS2* mRNA was detected slightly ($P = 0.041$) but statistically significantly upregulated in the SM-treated skin samples compared with that in the control, not-treated mice (Figure 14f). Therefore, it can be concluded that SM does not induce severe side effects or adverse events when applied topically to mouse skin, although optimal dosing of SM may be considered for repeated skin applications. These data are consistent with published reports indicating that no side effects or severe significant adverse events were recorded when SM was applied on the skin of animal models of human skin disease (Soleimani et al., 2019) as well as on skin patients with melasma (Altaei, 2012; Nofal et al., 2019) or breast cancers (Becker-Schiebe et al., 2011).

DISCUSSION

Epidermal homeostasis requires the orchestration of a series of key biological processes, such as spatiotemporal coordination of KC proliferation and differentiation, which are mediated to a large extent by soluble factors. It is now well-established that disruption of this balance is a hallmark of skin diseases, including psoriasis and atopic dermatitis (Goleva et al., 2019; Rendon and Schäkel, 2019). Therefore, it is of great interest to find modulators of epidermal homeostasis to better understand the molecular mechanisms governing this process and develop optimal strategies for treating and/or curing skin diseases. In this study, we searched for natural products as modulators of the TGF-β1/miR-21-5p pathway in KCs. The TGF-β1/miR-21-5p signaling

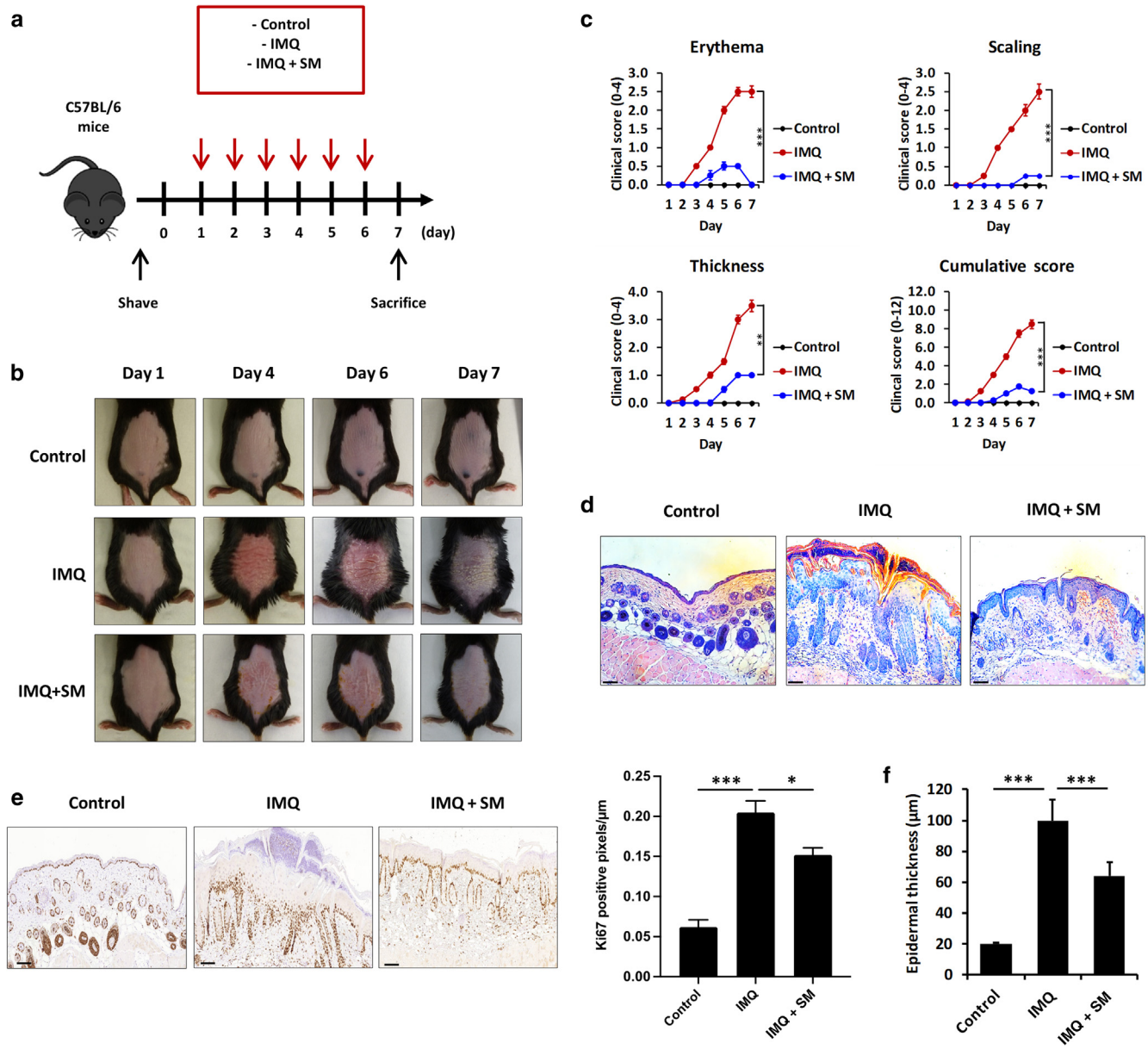

Figure 11. SM alleviates IMQ-induced psoriasis-like skin lesions in mice. (**a**) In vivo experimental flow chart. (**b**) Representative images of mice treated with acetone (control group), 5% IMQ cream (IMQ group), or 9 mg SM in acetone before 5% IMQ cream (IMQ + SM group) for 6 consecutive days. (**c**) PASI scores (erythema, scaling, and thickness) in all groups of mice were evaluated daily. The PASI cumulative score shows the severity of the inflammatory process. Statistical analyses were performed on day 7. (**d**) Representative images of H&E-stained sections of the back skin of mice collected on day 7. (**e**) Representative immunohistochemical detection of Ki-67 on sections of mouse back skin collected on day 7 (left panel). Bar = 100 µm. Quantification of Ki-67 staining intensity (pixels/µm) in the epidermis (right panel) of skin tissues collected on day 7. (**f**) Histological quantification of the epidermal thickness of skin tissues collected on day 7. Data are presented as the mean ± SEM of seven individual mice per group and are representative of one experiment performed twice. ANOVA test was used for **e** and **f** to test for significance between the different groups of mice. Repeated measures ANOVA test was used for **c**. $*P < 0.05$, $**P < 0.01$, and $***P < 0.001$. AMPK, AMP-activated protein kinase; CaCl2, clacium chloride; d, day; h, hour; IMQ, imiquimod; p-AMPK, phosphorylated AMP-activated protein kinase; PPARγ, peroxisome proliferator–activated receptor γ; SM, silymarin.

was chosen not only because it plays a pivotal role in KC proliferation, differentiation, and migration but also because its dysregulation has been reported in many skin disorders (Degueurce et al., 2016; Han et al., 2010; Li et al., 2013, 2004; Liu et al., 2016). Using the miR-ON RILES monitoring system, from a homemade library of plant extracts isolated from medicinal plants, we identified *C. asiatica* (L.), *M. caerulea* (L.), and *S. marianum* (L.) Gaertn crude extracts as positive regulators of TGF-β1/miR-21-5p signaling in HaCaT cells. We showed that SM, a mixture of structurally related flavonolignans that accounts for >80% of the *S. marianum* (L.) Gaertn. crude extract, was responsible for promoting miR-21-5p activity in TGF-β1–treated HaCaT cells. Using RNA immunoprecipitation assay combined with RT-qPCR, we showed that SM facilitates the loading of miR-21-5p into RISC machinery without affecting miR-21-5p expression levels, resulting in the downregulation of known miR-21-5p–target genes. We provided robust experimental

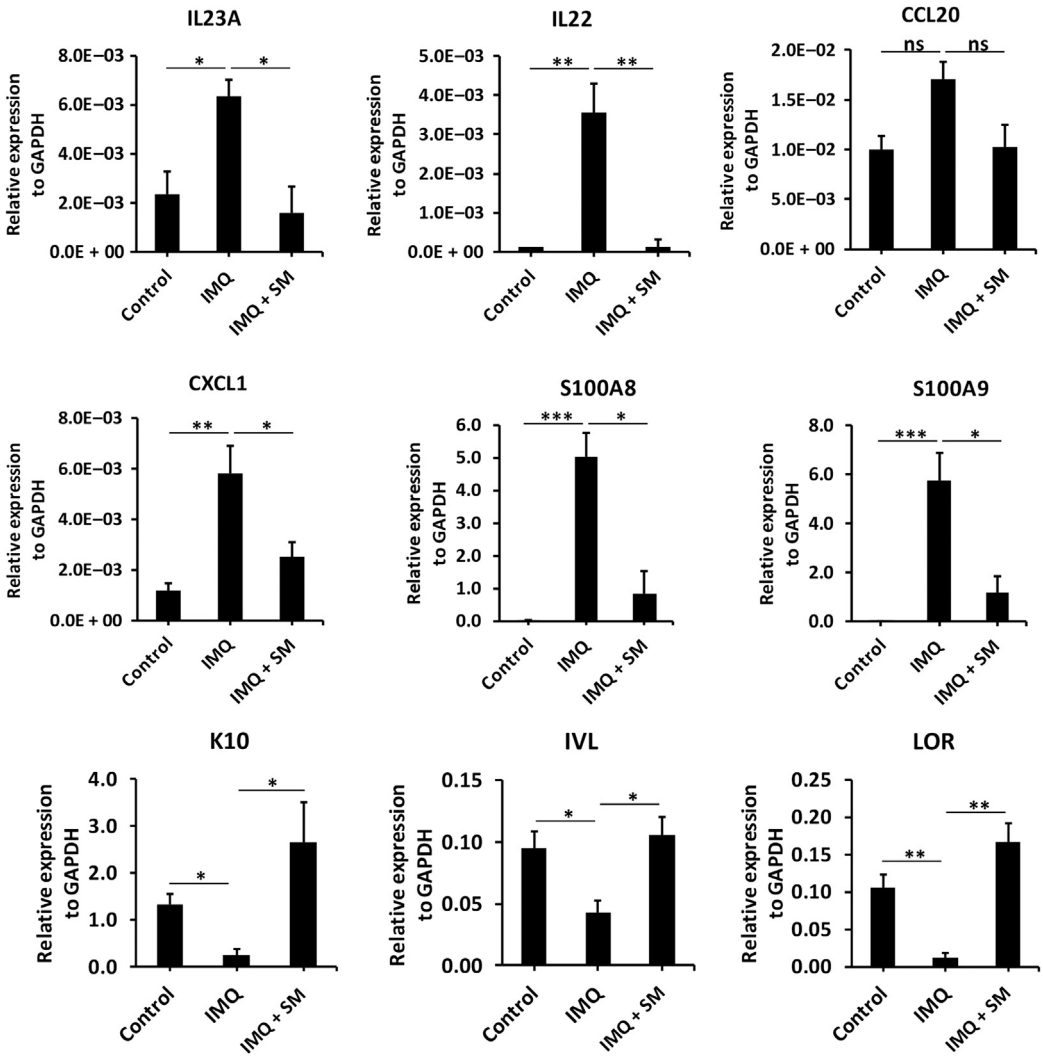

Figure 12. SM significantly reduces the mRNA levels of proinflammatory mediators and restores the gene expression levels of early and late markers of keratinocyte differentiation in the skin of IMQ-induced psoriasis mouse model. On day 7, dorsal skin samples from different groups of mice were collected to quantify the relative expression of *Il23a*, *Il22*, *Ccl20*, *Cxcl1*, *S100a8*, and *S100a9* to GAPDH levels by RT-qPCR. Data are presented as the mean ± SEM of seven individual animals per group and are representative of one experiment performed twice. ANOVA test was used to test for significance between the different groups of mice. $*P < 0.05$, $**P < 0.01$, and $***P < 0.001$. COX-2, cycloxygenase-2; IMQ, imiquimod; ns, not significant; SM, silymarin.

evidence that SM regulates KC proliferation, differentiation, as well as lipid synthesis through the activation of PPARγ and inhibition of NOTCH and AMPK/SREBP-1c signaling pathways. This extract also inhibits the inflammation response in KCs through the blockade of NF-κB signaling cascade. We finally reported for the first time that topical application of SM in the IMQ-induced psoriasis-like mouse model might represent a valuable alternative to attenuate and/or prevent psoriasis development.

The precise molecular mechanism responsible for the regulation of miR-21-5p activity by SM in HaCaT cells is not yet fully understood and needs further elucidation. Early studies have reported that only 60% of the miRNome is functional in cells (Flores et al., 2014; Lemus-Diaz et al., 2017; Mullokandov et al., 2012; Thomson et al., 2015) and that underestimating this feature might result in misinterpretation of biological roles of miRNA in cells (Ezzine et al., 2013; Flores et al., 2014; Jin et al., 2015; Simion et al., 2020). We (Simion et al., 2020) and others (Liu et al., 2005; Pitchiaya et al., 2019) have shown that a significant proportion of miRs localizes to cytosolic processing bodies (P-bodies) into the cells. By dissecting the dynamic localization of individual RNAs such as miRs, mRNAs, and long noncoding RNAs by intracellular single-molecule fluorescence microscopy, Pitchiaya et al. (2019) have recently shown that several miRs, including the miR-21-5p, are enriched at P-bodies in U2OS cell line. Although the role of miRs in these cytoplasmic foci is a matter of debate, growing evidence suggests that P-bodies act as a reservoir for unused miRs until the cytosolic RISC machinery becomes available again (Pitchiaya et al., 2019; Simion et al., 2020). Starting from the fact that the miR-21-5p displays a high basal expression in HaCaT cells (Ct value of 19 by RT-qPCR), which is further increased in response to TGF-β1 treatment, it is conceivable that a pool of miR-21-5p that is not incorporated into the RISC machinery might be transported to P-bodies for transient storage. It is then possible that SM might deviate the storage in P-bodies and so the delocalization of

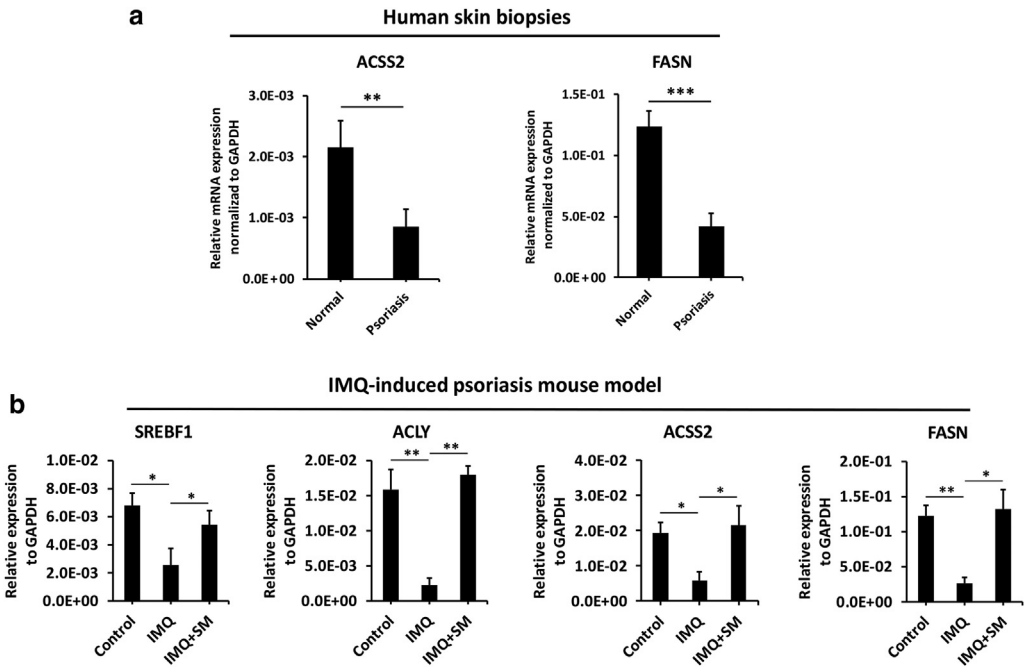

Figure 13. SM regulates the expression of genes involved in fatty acid and cholesterol biogenesis in the skin of IMQ-induced psoriasis mouse model. (**a**) RT-qPCR quantification of the relative expression of *ACSS2* and *FASN* to GAPDH levels in human skin biopsies from healthy (n = 10) and lesional skin of individuals with psoriasis (n = 9). (**b**) RT-qPCR quantification of the relative expression of *Srebf1*, *Acly*, *Acss2*, and *Fasn* to GAPDH levels in dorsal skin samples of mice collected on day 7 after treatment with acetone (control group), 5% IMQ cream (IMQ group), or 9 mg SM in acetone before 5% IMQ cream treatment (IMQ + SM group) for 6 consecutive days (n = 7 individual mice per group). Data are presented as the mean ± SEM of seven individual mice per group and are representative of one experiment performed twice. Two-tailed unpaired *t*-test was used for **a** to test for significance between healthy and lesional psoriatic skin samples. ANOVA test was used for **b** for multiple comparison between the different groups of mice. $*P < 0.05$, $**P < 0.01$, and $***P < 0.001$. IMQ, imiquimod; SM, silymarin.

miRs, either by direct physical interaction or in an indirect manner through a mediator(s) to be identified. As a result, although the total pool of miR-21-5p in cells remains the same, as detected by RT-qPCR (Figure 4b), the fraction of miR-21-5p processed by the cells to exert a negative post-transcriptional regulation on gene expression changes, as detected by the pRILES/21.5p probe throughout this study and proved by RNA immunoprecipitation assay and transcriptional analysis of miR-21-5p–target genes (Figure 4e). We do not exclude that other mechanisms could be involved and that will require a full program of work to be elucidated. Nevertheless, our results highlight again (Horvath et al., 2016; Lewis et al., 2017; Shan et al., 2008) the great potential of bioactive compounds for deciphering unrevealed molecular mechanisms occurring in living cells and show that the use of a functional monitoring system, such as the RILES, is an advantage for this purpose.

Only a few studies have examined the activity of SM in human KCs. Those studies have mainly focused their investigations on the protective role of SM against the harmful effects of UV (Fidrus et al., 2019; Katiyar et al., 2011; Svobodová et al., 2007). For example, Katiyar et al. (2011) have shown that SM promotes DNA repair in UVB-exposed KCs through the nucleotide excision repair pathway. In this study, we reported common biological properties of SM in in vitro–cultured human KCs and in a relevant mouse model of psoriasis.

We showed that SM inhibits the proliferation of HaCaT cells by blocking the cell cycle in the G0/G1 phase. Inhibitory effects of SM on cell proliferation have been reported in other cellular contexts, mainly cancer cells (Agarwal et al., 2003; Kim et al., 2019a; Varghese et al., 2005; Zi et al., 1998a, 1998b). For instance, Zi et al. (1998a) reported that SM induced G1 phase arrest through induction of the cyclin-dependent kinase inhibitor Cip1/p21 in human breast carcinoma. Our RNA-seq data tend to suggest that a similar event might also occur in KCs treated with SM. Downregulation of genes related to cell cycle progression, such as *CDK1*, *MKI67*, *PLK1*, and *CDC25A*, were detected in HaCaT cells treated with TGF-β1 plus SM. We confirmed significant downregulation of *CDC25A* in TGF-β1 plus SM–treated cells by RT-qPCR. However, unlike cancer cells (Kim et al., 2019a; Li et al., 2011a; Won et al., 2018), the treatment of HaCaT cells with SM did not induce apoptosis even after a long period of treatment (e.g., 9 days at the highest SM cell concentration, data not shown). We also showed, to our knowledge, the previously unreported ability of SM to block the early and late stages of KC differentiation by downregulating SMAD2/3 and NOTCH3 protein expression in HaCaT cells, while inducing at the same time the expression of lipogenic genes, such as *ACLY*, *ACSS2*, and *FASN*, resulting in lipid production in cells. These concomitant results are surprising because the differentiation of KCs is accompanied by an increase in lipid synthesis in cellulo and in vivo. Although we do not yet have a clear explanation of this process, we recently performed a high-performance liquid chromatography-tandem mass spectrometry analysis of lipids produced by the HaCaT cells in response to SM and

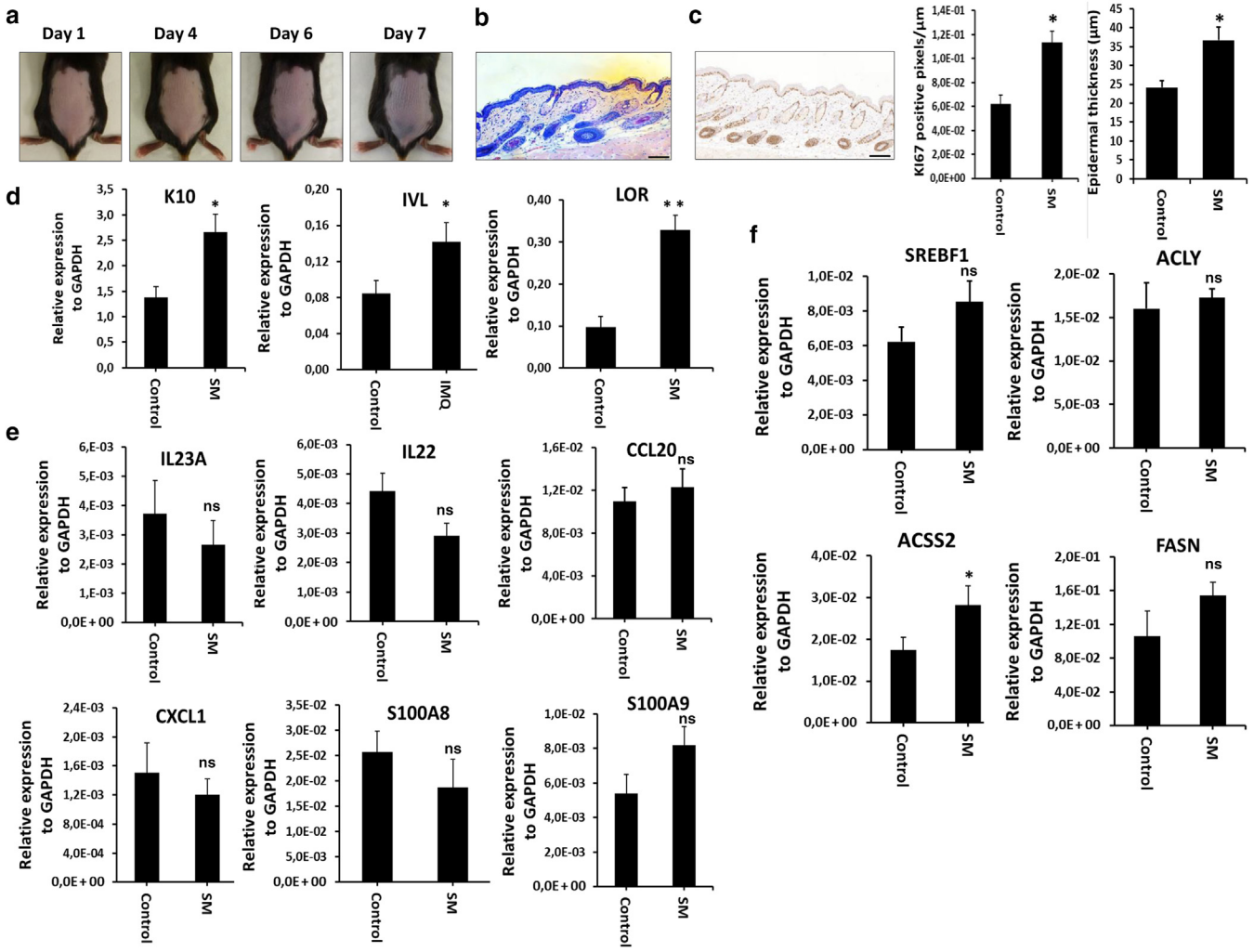

Figure 14. Evaluation of the safety and adverse events of topical application of SM on mice skin. SM (9 mg in acetone) was applied on the dorsal skin of mice (n = 7) for 6 consecutive days. Then mice were photographed on day 7 before collecting skin biopsy samples for histology and gene expression analysis. Control mice received no treatment (n = 7). (**a**) Representative pictures of one representative mouse treated with SM over time. (**b**) Representative H&E-stained tissue sections of the back skin of one representative mouse treated with SM. (**c**) Left panel: representative immunohistochemical detection of Ki-67 on tissue sections of mouse back skin of one representative mouse treated with SM. Right panel: quantification of Ki-67 staining intensity (pixels/µm) in the epidermis of SM-treated mice and control, not treated mice. RT-qPCR quantification of the relative expression of (**d**) epidermal differentiation, (**e**) inflammatory cytokines, as well as (**f**) lipogenic markers of SM-treated mice and control, not treated mice. Bar = 100 µM. Data in **c**, **d**, **e**, and **f** are the mean ± SEM of seven individual mice per group and are representative of one experiment. Two-tailed unpaired *t*-test was used to test for significance between SM-treated mice and control, not-treated mice. $*P < 0.05$ and $**P < 0.01$. IVL, involucrin; K, keratin; LOR, loricrin; ns, not significant; SM, silymarin.

found that SM stimulates the synthesis of ceramides and of phospholipids and conversely inhibits the synthesis of sterols and several fatty acids (data not shown). It is therefore likely that SM stimulates the synthesis of lipids found predominantly in not or poorly differentiated KCs in basal layers of the epidermis (Vietri Rudan and Watt, 2021) and in cells cultured in low calcium–containing media (Ponec et al., 1988). We are currently extending this finding. Nevertheless, we deciphered in part the underlying mechanisms responsible for lipid production in HaCaT cells. We showed that SM did not stimulate lipid metabolism in HaCaT cells through an AMPK/SREBP-1c–dependent mechanism but rather through an enhancement of the transcriptional activity of PPARγ (Varga et al., 2011). PPARγ is considered a major regulator of epidermal lipid metabolism. Topical treatment of hairless mouse skin with ciglitazone, a PPARγ agonist, has been shown to increase epidermal cholesterol, fatty acid, and ceramide biosynthesis and to accelerate lamellar body formation, secretion, and extracellular lipid processing after acute barrier disruption (Man et al., 2006). Other studies identified natural products from medicinal plants such as Honokiol from *Magnolia bark* and polyacetylene falcarindiol from *Notopterygium incisum* as PPAR agonists (Atanasov et al., 2013a, 2013b). Recently, Wölfle et al. (2017) have shown that the crude extract of *Gentiana lutea* activates PPARγ signaling pathway in KCs, resulting in increased expression of ceramide synthase 3, involved in the ceramide synthesis. We do not exclude that other signaling pathways might also contribute to lipid synthesis in HaCaT cells treated with SM in the presence of TGF-β1. This is supported by the observation that PPARγ reached a maximum activity when HaCaT cells were treated with TGF-β1 plus 31 µg/ml SM,

whereas the gene expression of *ACLY*, *ACSS2*, and *FASN* continued to increase when cells were treated with the highest of SM concentrations (e.g., 62 μg/ml plus TGF-β1) (Figure 9). In the last few years, several studies have shown that mTOR plays important roles in the regulation of lipid metabolism in response to insulin and nutrient availability (Laplante and Sabatini, 2009; Tang et al., 2016). In addition, MAPK/extracellular signal–regulated kinase and c-Jun N-terminal kinase signaling pathways are known to regulate lipid synthesis in several cell types (Greenberg et al., 2001; Gubern et al., 2009; Cristea et al., 2020). Another alternative candidate might also be ANGPTL4. ANGPTL4 plays a critical role in the lipid homeostasis of adipocytes by mediating the inhibition of the lipoprotein lipase, an enzyme that catalyzes the lipolysis of triglyceride-rich lipoproteins (Kersten et al., 2000; Sukonina et al., 2006). Interestingly, *ANGPTL4* is one of the most significantly upregulated genes in HaCaT cells treated with TGF-β1 plus SM (a 6.8-fold increase compared with that in cells treated with TGF-β1 alone, $P < 0.001$).

Previous studies have reported a decrease in free fatty acids and total ceramides content in lesional skin from patients with psoriasis compared with that in healthy skin, resulting in increased transepidermal water loss and default in skin remodeling (Chapkin et al., 1986; Motta et al., 1994, 1993; Nakajima et al., 2013). More recently, Tawada et al. (2014) have shown that the proportion of ceramides with long-chain fatty acids was significantly lower in the lesional skin of patients with psoriasis than in the skin of healthy volunteers. Similar observations have been reported in the epidermis of db/db mice with type 2 diabetes (Kim et al., 2019b). Consistent with our recent high-performance liquid chromatography-tandem mass spectrometry results indicating that SM stimulates the synthesis of ceramides and phospholipids in KCs, we postulated that topical administration of SM on the back skin of mice before IMQ application might correct this default. We first showed that *ACSS2* and *FASN* mRNA levels were significantly downregulated in the lesional skin of patients with psoriasis compared with those in healthy skin. We then clearly showed the preventive effect of SM against psoriasis using the IMQ-induced psoriasis mouse model. We showed that the reduced lipogenic gene expression in IMQ-treated mice is restored to normal levels by SM pretreatment, indicating that SM could improve the skin barrier function. Consequently, SM efficiently decreased epidermal thickness, parakeratosis, hyperkeratosis, and dermal-infiltrating cells. Moreover, SM induces the expression of KC differentiation markers (K10, IVL, and LOR) and inhibits the expression of proinflammatory cytokines (IL-23A and IL-22) as well as some mediators (CXCL10, CCL20, S100A8, and S100A9) involved in the pathogenesis of psoriasis. Recently, Wang et al. (2017) established a causal relationship between inflammation and KC differentiation. They reported that stimulation of HaCaT cells with IL-36γ, a cytokine highly expressed in active psoriatic lesions, induces the expression of markers for cell proliferation such as β-catenin, cyclin D1, and Ki-67, when on the contrary, it inhibits the expression of K1, IVL, and FLG. Others (Albanesi et al., 2018; Buerger et al., 2017) argued that KC hyperproliferation in psoriatic lesions could exacerbate the disruption of the balance between proliferation and differentiation. We revealed that SM treatment suppressed NF-κB activation in HaCaT cells stimulated with IL-22, a cytokine secreted by T helper 17 and T helper 22 cells and involved in KCs hyperproliferation (Eyerich et al., 2009). The antiproliferative effect of SM was further confirmed in vivo, as attested by a significant decrease in the percentage of Ki-67–positive cells in the epidermis of mice pretreated with SM before IMQ topical application. Therefore, it is likely that the predominant curative effect of SM in the IMQ-induced psoriasis mouse model should be more closely related to the inhibition of hyperproliferation of KCs and correction of lipids synthesis.

In summary, we report in this study that the screening of medicinal plant extracts library using the miR-ON RILES system placed under the control of the TGF-β1/miR-21-5p signaling in HaCaT cells is a relevant approach to identify novel modulators of epidermal homeostasis with a possible therapeutic application in psoriasis. We conducted a comprehensive study to delineate the roles of SM in the biological behavior of KCs and showed that this extract inhibits proliferation, differentiation, and inflammatory responses in KC, whereas it induces at the same time lipid synthesis. We identified some underlying mechanisms implicated in these SM-regulated biological processes and revealed that the topical application of SM might represent an alternative pharmacological approach to ameliorate the severity of psoriasis. Overall, our study provides a rational basis for further investigations into the underlying molecular mechanisms of SM on miR-21-5p biogenesis and lipid synthesis in KCs.

MATERIALS AND METHODS

Cell culture

The immortalized human KCs cell line HaCaT was purchased from AddexBio (San Diego, CA) (number T002000). HaCaT cells were maintained in DMEM with 4.5 g/l glucose with L-Glutamine (number BE12-604F, Lonza, Basel, Switzerland) supplemented with 10% fetal bovine serum (number F7524, Invitrogen, Waltham, MA) and 100 units/ml of penicillin and 100 μg/ml of streptomycin (number P0781, Sigma-Aldrich, St. Louis, MO). To obtain cells exhibiting a basal KC phenotype, HaCaT cells were cultured for at least 4 weeks in calcium-free DMEM (number 21068028, Gibco, Waltham, MA) supplemented with 10% fetal bovine serum (number F7524, Invitrogen), 2 mM glutamine (number 25030081, Gibco), 100 units/ml penicillin, 100 μg/ml streptomycin, and calcium chloride to a final concentration of 0.07 mM (low calcium medium). Cells were induced to differentiate by adding calcium chloride to the culture medium to a final concentration of 1.8 mM (HC-containing medium). The medium was changed every 3 days for different time periods (3, 6, or 9 days).

Cell-based bioluminescence screening assay using the RILES reporter system

To monitor the functionality of miR-21-5p in HaCaT cells, the miR-ON RILES reporter system (Ezzine et al., 2013; Simion et al., 2021, 2020, 2017) was used. As recently reported (Abdallah et al., 2021) and briefly described, four fully complementary block sequences specific to miR-21-5p were subcloned in the 3′ untranslated region of the CymR transcriptional repressor gene. The generated expression plasmid was called pRILES/21.5pT, whereas the control RILES plasmid that did not contain miR-targeting sequence was denoted

pRILES. Both plasmids were sequenced to ensure the integrity of the molecular construct. To monitor the functionality of endogenously expressed miR-21-5p in HaCaT cells using the RILES/21.5pT reporter system, the cells were seeded onto 24-well plates at 3.5×10^5 cells per well and transfected the following day with 2.5 µg of either the pRILES or the pRILES/21.5pT plasmids using the PTG1 transfection reagent (Polytheragene SAS, Evry, France [Gonçalves et al., 2014]) used at the DNA/polymer weight ratio of 1/4. After 4 hours of transfection, the medium was replaced with DMEM high glucose medium supplemented with 0.5% serum, and cells were cultured overnight. Then, the next day, cells were treated in the same medium containing TGF-β1 (0, 2, 10, and 20 ng/ml) (number T7039, Sigma-Aldrich). The expression of the Firefly luciferase reporter gene was monitored 24 hours later and normalized to protein content using a routine procedure as previously described (Ezzine et al., 2013; Simion et al., 2021, 2020, 2017). Data were finally expressed as luciferase fold induction relative to control cells transfected with the pRILES.

For the screening procedure, HaCaT cells were seeded at 7.5×10^4 cells/well in triplicate into 96-well black tissue culture plates with a clear flat bottom (number 6120096, Lumox, Cergy, France). The following day, 0.5 µg of either the pRILES or the pRILES/21.5pT plasmids were transfected in HaCaT cells with PTG1 (pDNA/polymer weight ratio of 1/6). After 4 hours of transfection, the medium was replaced with DMEM high glucose supplemented with 0.5% fetal bovine serum, and cells were cultured overnight. Then, the following day, cells were treated with 10 ng/ml recombinant human TGF-β1 (number T7039, Sigma-Aldrich) in the presence of plant extracts used at indicated cellular concentrations. Negative controls were treated with TGF-β1 and DMSO used at 0.1% final concentration. Bioluminescence signals emitted from the cells were quantified 24 hours later using an IVIS Lumina II imaging scanner (PerkinElmer, Waltham, MA) as previously described (Ezzine et al., 2013; Simion et al., 2021, 2020, 2017). Compounds identified in primary screening were further confirmed by a dose-response study in a 24-well plate as described previously (Ezzine et al., 2013; Simion et al., 2021, 2020, 2017).

Plant extract library

The plant extract library consisted of 37 extracts dissolved in DMSO (Table 1). Briefly, plants were grown and harvested at the Comité de Développement Horticole de la Région Centre-Val de Loire (Saint Cyr en Val, France) and the Laboratoire de Biologie des Ligneux et Grandes Cultures (UPRES EA 1207, INRA, Orléans, France). A total of 10 g of either crushed dried areal parts (leaves and stems) or seeds were extracted at the Institut de Chimie Organique et Analytique (UMR 7311, Orléans, France) using a mixture of ethanol:water (70:30, v/v) as a solvent for 1 hour at room temperature (RT) using ultrasound-assisted method. The supernatant was recovered and clarified at 10,000 r.p.m. for 15 minutes before drying the raw material under nitrogen flow. All dried crude extracts were dissolved in DMSO at the concentration of 100 mg/ml and stored at −20 °C until used. SM, a standardized extract from *S. marianum* (L.) Gaertn seeds, was purchased from Sigma-Aldrich (number S0292).

Cell viability assay

HaCaT cells were plated into 96-well plates at 2×10^4 cells/well. Cells were then starved for 24 hours in DMEM high glucose medium supplemented with 0.5% serum and were treated with plant extracts. After 24 hours, cell viability was assessed using the XTT cell proliferation kit II (number 11465015001, Roche, Basel, Switzerland) according to the manufacturer's instructions. Cells were incubated with the XTT solution at a final concentration of 0.3 mg/ml for 4 hours at 37 °C, and the absorbance of formazan product was measured at 470 nm using a Victor spectrophotometer (PerkinElmer).

RNA immunoprecipitation

HaCaT cells were lysed in polysome lysis buffer (100 mM potassium chloride, 5 mM magnesium chloride, 10 mM 4-[2-Hydroxyethyl]-1-piperazine ethanesulfonic acid, pH 7.0, 0.5% Triton, 1 mM dithiothreitol, protease inhibitor cocktail [number P8340, Sigma-Aldrich], 1% phenylmethylsulfonyl fluoride [number P7626, Sigma-Aldrich], 50 mM sodium fluoride [Sigma-Aldrich, number S1504], and 2 mM vanadyl ribonucleoside complexes solution [number 94742, Sigma-Aldrich]). Precleared protein lysate (5 mg) was incubated with 5 µg of anti-AGO2 antibody (number ab32381, Abcam, Cambridge, United Kingdom) on a rotator overnight at 4 °C. Magnetic protein G Dynabeads (number 10004D, 80 µl, Invitrogen) were added, and protein lysate was further incubated on the rotator for 5 hours at 4 °C. The beads were first washed four times with polysome lysis buffer to remove unbound proteins, followed by a second set of four washes with polysome lysis buffer containing 1 M urea to reduce nonspecific interactions. The washed beads were then incubated in polysome lysis buffer in the presence of 0.1% SDS and 30 µg proteinase K for 30 minutes at 50 °C before RNA fraction extraction using an acid-chloroform procedure. The aqueous phase was used to isolate miRs using mirVana miRNA Isolation Kit (number AM1560, Ambion Life Technology, Waltham, MA) following the manufacturer's instructions. The amount of AGO2-associated miRs was then quantified by RT-qPCR.

RNA extraction, reverse transcription, and quantitative real-time-PCR

For mRNA analysis, total RNA was isolated from HaCaT or from homogenized mouse and human skin biopsies using TRIzol reagent (Invitrogen). Then, 100 ng of total RNA was reverse transcribed using the RevertAid First Strand cDNA Synthesis Kit (number K1622, Thermo Fisher Scientific, Waltham, MA). The RT-qPCR products were generated from 100 ng of cDNAs of mRNA using Luna Universal qPCR Master Mix (number M3003, New England Biolabs, Ipswich, MA) and gene-specific primers pairs listed in Table 2. For miR analysis, miRs were isolated from HaCaT cells using mirVana miRNA Isolation Kit (number AM1560, Ambion Life Technology) following the manufacturer's instructions. Then, 2 µl of miRs were reverse transcribed using the TaqMan Advanced miRNA cDNA Synthesis Kit (number A28007, Applied Biosystems, Waltham, MA). The resulting cDNA samples were preamplified using the Universal miR-Amp primers (number A28007, Applied Biosystems) to improve the detection of low-expressing miRs. The RT-qPCR products were generated from amplified cDNAs of miRs diluted to 1/10 (vol/vol) in RNase-free water using Luna Universal qPCR Master Mix (number M3003, New England Biolabs) and specific primer pairs to pri-miR-21 and pre-miR-21 listed in Table 2 and to hsa-miR-21-5p (number 000397) and hsa-miR-16-5p (number 000391) purchased from Applied Biosystems (TaqMan microRNA assays). RT-qPCR raw data were collected on the LightCycler 480 detection system (Roche Applied Science, Indianapolis, IN). mRNA expression was related to the expression of the housekeeping gene *GAPDH*, whereas miR

expression was related to the expression of miR-16-5p. The relative expression levels of miRs and mRNAs were determined using the standard $2^{-\Delta\Delta}$CT Livak and Schmittgen method (Livak and Schmittgen, 2001).

RNA-seq analysis

Total RNA from HaCaT cells treated with TGF-β1 (10 ng/ml) in the presence or absence of SM (31 μg/ml) was isolated using mirVana miRNA Isolation Kit (number AM1560, Ambion Life Technology) and evaluated using a Bioanalyzer 2100 (Agilent Technologies, Santa Clara, CA). Libraries were generated from 0.5 μg of total RNA using the Illumina TruSeq Stranded mRNA Library Prep Kit according to the manufacturer's instructions. This work has benefited from the facilities and expertise of the high-throughput sequencing core facility of I2BC (Centre de Recherche de Gif; http://www.i2bc.paris-saclay.fr/). Libraries were sequenced on the Illumina NextSeq 500 Sequencing System using paired-end 100-bp runs. Image analysis, base calling, and demultiplexing were performed using RTA 2.4.6 and bcl2fastq 2.18.12. The raw reads were trimmed with Cutadapt-1.15. Only reads longer than 10 bp were kept for analysis. Sequences were aligned to the human genome hg19 with TopHat2 2.1.1 using default parameters. Uniquely mapped reads were assigned to genes with FeatureCounts (Subread, version 1.5.2). Differential expression analysis was performed with DESeq2 package in R. Differentially expressed transcripts were analyzed by Gene Ontology enrichment and Kyoto Encyclopedia of Genes and Genomes pathway to identify possible enrichment of genes with specific biological pathways. The clusterProfiler package in R was used for the analysis.

Cell cycle analysis

HaCaT cells were plated in six-well plates at 6×10^5 cells/well before treatment with SM for 24 hours. Then, the cells were harvested by trypsinization, washed in cold PBS, and fixed in cold 70% ethanol for 2 hours at −20 °C. After being washed twice with PBS, cells were then suspended in PBS containing RNase A (100 μg/ml) for 30 minutes at 37 °C. Cell permeabilization was performed with 0.2% Triton X-100 in PBS for 10 minutes at RT. Finally, the cells were stained with 10 μl of stock propidium iodide solution (1 mg/ml in PBS) for 15 minutes at 37 °C. The cell cycle distribution was determined using a BD FACSort flow cytometer (BD, Franklin Lakes, NJ). The percentages of cells in each cell cycle phase were analyzed using BD CellQuestTM Pro Software (BD).

In vitro scratch wound healing assay

HaCaT cells were cultured into a 24-well plate to achieve 100% confluence. Confluent cell monolayers were then starved in DMEM high glucose medium supplemented with 0.5% serum for 24 hours. The cell monolayers were then scratched with a 1,000 μl sterile pipette tip across the center of the wells, washed two times with PBS, and finally treated with TGF-β1 (10 ng/ml) in the presence or absence of SM (31 μg/ml) in DMEM high glucose medium supplemented with 0.5% serum. The cell migration was immediately followed in real time by video microscopy using a Zeiss Axiovert 200 M (Carl Zeiss, White Plains, NY) fully motorized microscope equipped with a thermostatic incubation chamber at 37 °C and 5% carbon dioxide. The scratched regions were photographed automatically every 2 hours for 2 days. Wound areas at individual time points were analyzed using the ZEN LE Digital Imaging Software (Carl Zeiss). Data were expressed as the percentage of closure by normalizing the calculated area to 100% of the wound area of untreated cells.

UVB irradiation

HaCaT cells were plated into 24-well plates at 2.5×10^4 cells/well and then starved in DMEM high glucose medium supplemented with 0.5% serum for 24 hours before treating the cell monolayers for 6 hours at 37 °C and 5% carbon dioxide with different concentrations of SM (15, 31, and 62 μg/ml) prepared in DMEM high glucose medium supplemented with 0.5% serum. After two washes in PBS, the cells in PBS were irradiated with UVB (100 mJ/cm2) using a solar simulator (Vilber Lourmat, Collégien, France). Nonirradiated cells were used as control. After UVB irradiation, PBS was removed, and the cells were incubated at 37 °C for 16 hours with different concentrations of SM (15, 31, and 62 μg/ml) prepared in DMEM high glucose medium supplemented with 0.5% serum. After incubation, monolayer cells were washed in PBS and lysed in ice-cold RIPA buffer for western blot analysis.

Western blot

Cells were lysed in ice-cold RIPA buffer (number 89901, Thermo Fisher Scientific) supplemented with 1% protease inhibitor cocktail (number P8340, Sigma-Aldrich), 1% phenylmethylsulfonyl fluoride (number P7626, Sigma-Aldrich), and 50 mM sodium fluoride (number S1504, Sigma-Aldrich). Protein concentrations were quantified by BCA protein assay kit (number UP40840A, Interchim, Montluçon, France), and samples containing equal amounts of protein were then resolved on 10% SDS-PAGE gel before being electro-transferred onto a polyvinylidene difluoride membrane for western blotting analysis. After a blocking step with 5% (w/v) nonfat dry milk for 1 hour at RT, membranes were incubated overnight at 4 °C with antibodies specific to AGO2 (1:1,000, number ab32381, Abcam), AMPKα1/2 (1:500, number ab80039, Abcam), phosphorylated Thr183/172-AMPKα1/2 (1:1,000, number sc-101630, Santa Cruz Biotechnology, Dallas, TX), β-actin (1:5,000, number A2066, Sigma-Aldrich), cyclooxygenase 2 (1:500, number 12282T, Cell Signaling Technology, Danvers, MA), cytokeratin 1 (1:500, number ab93652, Abcam), cytokeratin 10 (1:500, number ab9025, Abcam), GAPDH (1:5,000, number ab9485, Abcam), IVL (1:1,000, number I9018, Sigma Aldrich), LOR (1:500, number ab24722, Abcam), NOTCH3 (1:1,000, number 5276S, Cell Signaling Technology), SMAD2/3 (1:1,000, number 3102S, Cell Signaling Technology), phosphorylated Ser465/467-SMAD2 (1:1,000, number 3108S, Cell Signaling Technology), and SREBP-1 (1:250, number sc-13551, Santa Cruz Biotechnology). The Enhanced chemiluminescence kit was used to reveal bands of interest. Bio-Rad Gel imaging system and ImageJ software (National Institutes of Health, Bethesda, MD) were employed to quantify luminescence signals from protein bands. The relative expression of each target protein was normalized to β-actin or GAPDH protein expression.

Immunofluorescence staining

HaCaT cells plated on 24-well plates containing glass coverslips were treated with SM or all-trans retinoic acid at indicated concentrations for 9 days. Cell monolayers were then fixed with 4% paraformaldehyde for 15 minutes at RT and permeabilized in a 1% BSA, 10% fetal bovine serum, 0.3 M glycine, and 0.1 % Triton X-100 PBS solution for 1 hour at RT. HaCaT cells were stained with anti-cytokeratin 10 antibody (1:100, number 9025, Abcam) overnight at 4 °C, followed by incubation with an Alexa Fluor 488 goat anti-mouse IgG (H+L) (number A-10680, Invitrogen). After PBS

Table 2. List of Primers for RT-qPCR

Genes	Species	Sequences (5′–3′)
CDC25A	Human	F: TACATTCCCTACCTCAGAAGCTG R: GCAGCCACGAGATACAGGTC
IGFBP3	Human	F: GCCAGCGCTACAAAGTTGAC R: ATGTGTACACCCCTGGGACT
PDCD4	Human	F: TGACTCTCTCTTTTCCGGTGA R: GTCCCGGGATGAGTTTTTCCT
GAPDH	Human	F: CCAAAAGGGTCATCATCTC R: GGCCATCCACAGTCTTCT
IVL	Human	F: TGAAACAGCCAACTCCAC R: TTCCTCTTGCTTTGATGGG
K1	Human	F: GATTGCCACCTACAGGACCC R: ACAGACACACTCACGTTCGG
K10	Human	F: GCATGGCAACTCACATCAGG R: CAGCCTGGCATTGTCGATCT
FLG	Human	F: GGATGAAGCCTATGACACCACT R: AACTCTGGATCCCCTACGCT
LOR	Human	F: ACGTCTCCTCGCAGCAGG R: CTATTTGGACGGCCAGGT
NOTCH1	Human	F: GAATGGCGGGAAGTGTGAAGC R: TAGTCTGCCACGCCTCTGC
NOTCH2	Human	F: TACAGTTGTCGCTGCTTGCC R: CGACGAAGGTTTCACAGTGC
NOTCH3	Human	F: AGGGACGTCAGTGTGAACTC R: GTCCACATCCTGCTGGCATC
ACLY	Human	F: TGAGGAAGCATCCGGAGGTA R: TCCGATGATGGTCACTCCCT
ACSS2	Human	F: CAGGAGGAAGCTGGAGCC R: GGTGCAGCTCGCGGTAG
FASN	Human	F: TCGTGGGCTACAGCATGGT R: GCCCTCTGAAGTCGAAGAAGAA
GAPDH	Human	F: CCAAAAGGGTCATCATCTC R: GGCCATCCACAGTCtTCT
Pri-miR-21	Human	F: TTTTGTTTTGCTTGGGAGGA R: AGCAGACAGTCAGGCAGGAT
Pre-miR-21	Human	F: TGTCGGGTAGCTTATCAGAC R: TGTCAGACAGCCCATCGACT
IVL	Mouse	F: CACCAGGAGTGTCAGGAACC R: CAGTTCTGGTTCAGGTGGCT
K10	Mouse	F: AGTGGTACGAGAAGCATGGC R: GCACGTTGGCATTGTCAGTT
LOR	Mouse	F: AACAGTATCAGTGCCAGAGC R: TCTGACTGGTCTGCTGAGAG
SREBF1	Mouse	F: GGAACAGACACTGGCCGAGA R: CGGGAAGTCACTGTCTTGGTT
ACLY	Mouse	F: CAGCTATGCCCCAAGGAAAGA R: CGTCTCGGGAACACACGTAG
ACSS2	Mouse	F: GGGATCATGCGCACAGTCTA R: AAGTGCCGATTCCACCTCTG
FASN	Mouse	F: CTGTGCCCGTCGTCTATACC R: AACCTGAGTGGATGAGCACG
IL23A	Mouse	F: AGCAACTTCACACCTCCCTAC R: ACTGCTGACTAGAACTCAGGC
IL22	Mouse	F: TCCAGCAGCCATACATCGTC R: CCTCGGAACAGTTTCTCCCC
CCL20	Mouse	F: AGGCAGAAGCAGCAAGCAAC R: CAAGCTTCATCGGCCATCTG
CXCL1	Mouse	F: GACCATGGCTGGGATTCACC R: CGCGACCATTCTTGAGTGTG
S100A8	Mouse	F: AAATCACCATGCCCTCTACAAG R: CCCACTTTTATCACCATCGCAA
S100A9	Mouse	F: CACCCTGAGCAAGAAGGAAT R: TGTCATTTATGAGGGCTTCATTT
GAPDH	Mouse	F: CCAAAAGGGTCATCATCTC R: GGCCATCCACAGTCTTCT

Abbreviations: F, female; IVL, involucrin; K, keratin; LOR, loricrin; M, male.

washing, coverslips were mounted using the VECTASHIELD Antifade Mounting Medium containing DAPI to stain the cell nuclei in blue (number H-1200, Vector Laboratories, Burlingame, CA). Slides were analyzed with Zeiss Axiovert 200M microscope (Carl Zeiss).

Lipid detection

Lipid droplets were stained in HaCaT cells using the Lipid (Oil Red O) Staining Kit (number MAK194, Sigma-Aldrich). Briefly, SM-treated cells were washed with PBS and fixed for 30 minutes at RT with 10% formalin solution. Cells were then incubated with filtered Oil Red O (60 mg in 20 ml isopropanol solution diluted 3:2 with water) for 20 minutes at RT. Stained cells were washed in distilled water, counterstained with hematoxylin, and visualized by optical microscopy equipped with a color CDD imaging system.

NF-κB and PPAR luciferase reporter assays

HaCaT cells were transfected with 2.5 μg pNF-κB-luc reporter plasmid (number 631743, Clontech Laboratories, Mountain View, CA) or PPRE X3-TK-luc plasmid (number 1015, Addgene, Watertown, MA) using the PTG1 transfection reagent (Polytheragene SAS, Evry, France) at DNA/polymer weight ratio of 1/4 as described earlier. The cells were then treated with recombinant human IL-22 (50 ng/ml, number 782-IL010, R&D Systems, San Diego, CA) or recombinant human TGF-β1 (10 ng/ml, number T7039, Sigma-Aldrich) with or without SM at indicated concentrations for 24 hours. Firefly luciferase activity in cells was monitored and normalized to total protein as described earlier.

ELISA

HaCaT cells were treated with TNF-α (1 ng/ml) with or without SM at indicated concentrations for 24 hours. Secreted IL-6 levels in the culture medium were quantified using the DuoSet ELISA kit (number DY206, R&D Systems) according to the manufacturer's instructions.

Mice and in vivo treatments

Female C57BL6/JRj mice (aged 8–10 weeks) were purchased from Janvier Labs (Saint Berthevin, France). All experiments were carried out in strict accordance with the rules of the French Ministry of Agriculture and the European Communities Council Directive (86/609/EEC). Experimental procedures were approved by a local ethical committee (Comité d'Ethique pour l'Expérimentation Animale, Campus d'Orléans [French Registration CECCO 03]). Mice were shaved on the back skin, randomly divided into three groups of seven mice each, and then topically treated with either 200 μl acetone alone (control group) or 62.5 mg IMQ from a commercially available cream (Aldara 5%, 3M Pharmaceuticals, Saint Paul, MN) (IMQ group) or 9 mg SM in 200 μl acetone for 45 minutes before the IMQ treatment (IMQ + SM) once daily for 6 consecutive days. On

the seventh day, all the mice were killed, and their skin was collected for further analysis.

Scoring the severity of psoriatic skin lesion

The severity of the skin lesion was graded by PASI as previously mentioned (Abdallah et al., 2021). Briefly, the skin erythema, scaling, and thickness were scored independently from 0 to 4 (0, none; 1, slight; 2, moderate; 3, marked; and 4, severe), and the total score was applied to measure the severity of inflammation (score range = 0–12).

Histopathological and immunohistochemistry analysis

Skin samples from each mouse were fixed in 10% neutral-buffered formalin for not more than 24 hours and then embedded in paraffin. The samples were cut into 6-μm sections, stained with H&E, and observed under Zeiss Axiovert 200M microscope (Carl Zeiss) equipped with a color camera. For immunohistochemical staining, the skin sections were incubated with anti–Ki-67 antibody (1:200, number ab16667, Abcam) in PBS with 3% BSA for 1 hour at RT. Then, sections were incubated with a goat biotinylated antirabbit secondary antibody (BP-9100-50, Vector Laboratories) for 30 minutes at RT, followed by incubation with avidin/horseradish peroxidase complex (Vector Laboratories) for 30 minutes. To reveal staining, 3,3′-diaminobenzidine (Vector Laboratories) was applied to sections for 5 minutes, which forms a brown color when oxidized in a reaction catalyzed by horseradish peroxidase. Finally, nuclei were counterstained with hematoxylin for 5 minutes. After staining, sections were mounted with a coverslip and mounting medium. Images were obtained with a Panoramic Slides Scanner and scanned at ×40 magnification. On each skin section, three representative areas were delimited on the program CaseViewer in the zone of interest (the epidermis). The number of Ki-67–positive nuclei was quantified in each zone with the Nucleo-Quant feature of the Quantcenter plug-in and normalized to the length of each zone in micrometers. Epidermis thickness was determined by taking three measurements on each section.

Patients and biopsies

A total of 4-mm punch biopsies were collected from the lesional skin of eight patients with psoriasis (five women and three men, with ages ranging from 18 to 60 years) at the Centre Hospitalier Régional d'Orléans (Orléans, France). Furthermore, 6-mm punch biopsies, collected from nine healthy donors (nine women with ages ranging from 41 to 60 years), were obtained from the Laboratoire BIO-EC (Longumeau, France).

Ethical approval

All procedures performed in studies involving human participants were in accordance with the ethical standards of the French National Research Agency committee, in compliance with French laws L. 1123-7. The study was approved by the Bioethics Committees of the Centre Hospitalier Régional d'Orléans and the Sub-Mediterranean II committee (Comité de Protection des Personnes). The study is referenced under the identification number 2017-A03036-47, with written informed consent from the participants.

Statistical analysis

All data are expressed as mean values ± SEM. Statistical analyses were performed using GraphPad Prism 8 (GraphPad Software, San Diego, CA). Normal distribution of data was first evaluated using Shapiro–Wilk test. Parametric two-tailed unpaired Student *t*-tests were used for comparison between two groups of samples, and one-way ANOVA with Tukey posthoc test was used for the comparison between several groups of samples (e.g., >2). ANOVA test with repeated measurement method coupled with Geisser Greenhouse correction and the Tukey posthoc test was used for multiple comparison between groups of samples collected at several time points. For RNA-seq data, the $\log_2$ fold change for a given gene was determined by taking the ratio of the mean of the normalized read counts in the TGF plus SM–treated group to the TGF-β1 control group, followed by a $\log_2$ transformation to obtain a normal to near-normal distribution. The *P*-value of each gene was determined by the Wald test, and the false discovery rate was calculated using the Benjamini–Hochberg method (Benjamini and Hochberg, 1995) to adjust the *P*-value for multiple testing. To find out the significant DEGs, we have applied an absolute $\log_2$ fold change cutoff of 1 and an adjusted *P*-value of 0.01.

Data availability statement

RNA-sequencing data have been deposited (accession number GSE162336) in the National Center for Biotechnology Information Gene Expression Omnibus database (http://www.ncbi.nlm.nih.gov/geo/).

ORCIDs

Elodie Henriet: http://www.orcid.org/0000-0002-1563-9486
Florence Abdallah: http://www.orcid.org/0000-0002-9810-2528
Yoan Laurent: http://www.orcid.org/0000-0002-0411-1950
Cyril Guimpied: http://www.orcid.org/0000-0002-2612-9190
Emily Clement: http://www.orcid.org/0000-0001-6027-6488
Michel Simon: http://www.orcid.org/0000-0003-3655-6329
Chantal Pichon: http://www.orcid.org/0000-0003-3161-3937
Patrick Baril: http://www.orcid.org/0000-0001-8290-9899

CONFLICT OF INTEREST

The authors state no conflict of interest.

ACKNOWLEDGMENTS

We thank our colleagues from the VALBIOCOSM consortium for the preparation of the medicinal plant library: Benoit Maunit (Institut de Chimie Organique et Analytique, UMR 7311, Orléans, France), Emilie Destandau (Institut de Chimie Organique et Analytique, UMR 7311), Sophie Bresch (Comité de Développement Horticole de la Région Centre-Val de Loire, Saint Cyr en Val, France), and Christophe Hano (Laboratoire de Biologie des Ligneux et Grandes Cultures, UPRES EA 1207, INRA, Orléans, France). The funding was attributed to PB by the ARD (Ambition, Research and Development) 2020 program led by the University of Orleans and supported by the Region Centre-Val de Loire and the European Regional Development Fund program (University of Orleans is funded by the Region Centre-Val de Loire). ED (PhD fellow) and YL (Scientific manager) were funded by the ARD 2020 program.

AUTHOR CONTRIBUTIONS

Conceptualization: EH, PB; Funding Acquisition: PB; Methodology: EH, FA, YL, CG, EC; Project Administration: PB; Supervision: MS, CP, PB; Visualization: EH, PB; Writing - Original Draft Preparation: EH, PB; Writing - Review and Editing: EH, MS, CP, PB

REFERENCES

Aashaq S, Batool A, Mir SA, Beigh MA, Andrabi KI, Shah ZA. TGF-β signaling: A recap of SMAD-independent and SMAD-dependent pathways. J Cell Physiol 2022;237:59–85.

Abdallah F, Henriet E, Suet A, Arar A, Clemençon R, Malinge JM, et al. miR-21-3p/IL-22 axes are major drivers of psoriasis pathogenesis by modulating keratinocytes proliferation-survival balance and inflammatory response. Cells 2021;10:2547.

Agarwal C, Singh RP, Dhanalakshmi S, Tyagi AK, Tecklenburg M, Sclafani RA, et al. Silibinin upregulates the expression of cyclin-dependent kinase inhibitors and causes cell cycle arrest and apoptosis in human colon carcinoma HT-29 cells. Oncogene 2003;22:8271–82.

Albanesi C, Madonna S, Gisondi P, Girolomoni G. The interplay between keratinocytes and immune cells in the pathogenesis of psoriasis. Front Immunol 2018;9:1549.

Altaei T. The treatment of melasma by silymarin cream. BMC Dermatol 2012;2:12–8.

Atanasov AG, Blunder M, Fakhrudin N, Liu X, Noha SM, Malainer C, et al. Polyacetylenes from Notopterygium incisum–new selective partial agonists of peroxisome proliferator-activated receptor-gamma. PLoS One 2013a;8:e61755.

Atanasov AG, Wang JN, Gu SP, Bu J, Kramer MP, Baumgartner L, et al. Honokiol: a non-adipogenic PPARγ agonist from nature. Biochim Biophys Acta 2013b;1830:4813–9.

Atanasov AG, Zotchev SB, Dirsch VM. International Natural Product Sciences Taskforce, Supuran CT. Natural products in drug discovery: advances and opportunities. Nat Rev Drug Discov 2021;20:200–16.

Becker-Schiebe M, Mengs U, Schaefer M, Bulitta M, Hoffmann W. Topical use of a silymarin-based preparation to prevent radiodermatitis : results of a prospective study in breast cancer patients. Strahlenther Onkol 2011;187:485–91.

Benjamini Y, Hochberg Y. Controlling the false discovery rate: A practical and powerful approach to multiple testing. J R Stat Soc 1995;57:289–300.

Bhowmick NA, Ghiassi M, Bakin A, Aakre M, Lundquist CA, Engel ME, et al. Transforming growth factor-β1 mediates epithelial to mesenchymal transdifferentiation through a RhoA-dependent mechanism. MBoC. Mol Biol Cell 2001;12:27–36.

Blanpain C, Fuchs E. Epidermal stem cells of the skin. Annu Rev Cell Dev Biol 2006;22:339–73.

Borowiec AS, Delcourt P, Dewailly E, Bidaux G. Optimal differentiation of in vitro keratinocytes requires multifactorial external control. PLoS One 2013;8:e77507.

Buerger C, Shirsath N, Lang V, Berard A, Diehl S, Kaufmann R, et al. Inflammation dependent mTORC1 signaling interferes with the switch from keratinocyte proliferation to differentiation. PLoS One 2017;12:e0180853.

Buschke S, Stark H-J, Cerezo A, Prätzel-Wunder S, Boehnke K, Kollar J, et al. A decisive function of transforming growth factor-β/Smad signaling in tissue morphogenesis and differentiation of human HaCaT keratinocytes. Mol Biol Cell 2011;22:782–94.

Candi E, Schmidt R, Melino G. The cornified envelope: a model of cell death in the skin. Nat Rev Mol Cell Biol 2005;6:328–40.

Chapkin RS, Ziboh VA, Marcelo CL, Voorhees JJ. Metabolism of essential fatty acids by human epidermal enzyme preparations: evidence of chain elongation. J Lipid Res 1986;27:945–54.

Chendrimada TP, Gregory RI, Kumaraswamy E, Norman J, Cooch N, Nishikura K, et al. TRBP recruits the Dicer complex to Ago2 for microRNA processing and gene silencing. Nature 2005;436:740–4.

Cristea S, Coles GL, Hornburg D, Gershkovitz M, Arand J, Cao S, et al. The MEK5-ERK5 kinase axis controls lipid metabolism in small-cell lung cancer. Cancer Res 2020;80:1293–303.

Davies M, Robinson M, Smith E, Huntley S, Prime S, Paterson I. Induction of an epithelial to mesenchymal transition in human immortal and malignant keratinocytes by TGF-beta1 involves MAPK, Smad and AP-1 signalling pathways. J Cell Biochem 2005;95:918–31.

Davis BN, Hilyard AC, Lagna G, Hata A. SMAD proteins control DROSHA-mediated microRNA maturation. Nature 2008;454:56–61.

Davis BN, Hilyard AC, Nguyen PH, Lagna G, Hata A. Smad proteins bind a conserved RNA sequence to promote microRNA maturation by drosha. Mol Cell 2010;39:373–84.

Degueurce G, D'Errico I, Pich C, Ibberson M, Schütz F, Montagner A, et al. Identification of a novel PPARβ/δ/miR-21-3p axis in UV-induced skin inflammation. EMBO Mol Med 2016;8:919–36.

Denli AM, Tops BBJ, Plasterk RHA, Ketting RF, Hannon GJ. Processing of primary microRNAs by the microprocessor complex. Nature 2004;432:231–5.

Derynck R, Zhang YE. Smad-dependent and Smad-independent pathways in TGF-beta family signalling. Nature 2003;425:577–84.

Elsholz F, Harteneck C, Muller W, Friedland K. Calcium–a central regulator of keratinocyte differentiation in health and disease. Eur J Dermatol 2014;24:650–61.

Eyerich S, Eyerich K, Pennino D, Carbone T, Nasorri F, Pallotta S, et al. Th22 cells represent a distinct human T cell subset involved in epidermal immunity and remodeling. J Clin Invest 2009;119:3573–85.

Ezzine S, Vassaux G, Pitard B, Barteau B, Malinge JM, Midoux P, et al. RILES, a novel method for temporal analysis of the in vivo regulation of miRNA expression. Nucleic Acids Res 2013;41:e192.

Fidrus E, Ujhelyi Z, Fehér P, Hegedűs C, Janka EA, Paragh G, et al. Silymarin: friend or foe of UV exposed keratinocytes? Molecules 2019;24:E1652.

Flora P, Ezhkova E. Regulatory mechanisms governing epidermal stem cell function during development and homeostasis. Development 2020;147:dev194100.

Flores O, Kennedy EM, Skalsky RL, Cullen BR. Differential RISC association of endogenous human microRNAs predicts their inhibitory potential. Nucleic Acids Res 2014;42:4629–39.

Frankova J, Juranova J, Biedermann D, Ulrichova J. Influence of silymarin components on keratinocytes and 3D reconstructed epidermis. Toxicol In Vitro 2021;74:105162.

Frederick JP, Liberati NT, Waddell DS, Shi Y, Wang XF. Transforming growth factor β-mediated transcriptional repression of c-myc is dependent on direct binding of Smad3 to a novel repressive Smad binding element. Mol Cell Biol 2004;24:2546–59.

Goleva E, Berdyshev E, Leung DYM. Epithelial barrier repair and prevention of allergy. J Clin Invest 2019;129:1463–74.

Gonçalves C, Gross F, Guégan P, Cheradame H, Midou P. A robust transfection reagent for the transfection of CHO and HEK293 cells and production of recombinant proteins and lentiviral particles - PTG1. Biotechnol J 2014;9:1380–8.

Gonzales KAU, Fuchs E. Skin and its regenerative powers: an alliance between stem cells and their niche. Dev Cell 2017;43:387–401.

Greenberg AS, Shen WJ, Muliro K, Patel S, Souza SC, Roth RA, et al. Stimulation of lipolysis and hormone-sensitive lipase via the extracellular signal-regulated kinase pathway. J Biol Chem 2001;276:45456–61.

Griffiths CE, Barker JN. Pathogenesis and clinical features of psoriasis. Lancet 2007;370:263–71.

Guan Y, Yang YJ, Nagarajan P, Ge Y. Transcriptional and signalling regulation of skin epithelial stem cells in homeostasis, wounds and cancer. Exp Dermatol 2021;30:529–45.

Gubern A, Barceló-Torns M, Barneda D, López JM, Masgrau R, Picatoste F, et al. JNK and ceramide kinase govern the biogenesis of lipid droplets through activation of group IVA phospholipase A2. J Biol Chem 2009;284:32359–69.

Guinea-Viniegra J, Jiménez M, Schonthaler HB, Navarro R, Delgado Y, Concha-Garzón MJ, et al. Targeting miR-21 to treat psoriasis. Sci Transl Med 2014;6:225re1.

Hagiwara K, Gailhouste L, Yasukawa K, Kosaka N, Ochiya T. A robust screening method for dietary agents that activate tumour-suppressor microRNAs. Sci Rep 2015;5:14697.

Han G, Williams CA, Salter K, Garl PJ, Li AG, Wang XJ. A role for TGFbeta signaling in the pathogenesis of psoriasis. J Invest Dermatol 2010;130:371–7.

Hawley SA, Davison M, Woods A, Davies SP, Beri RK, Carling D, et al. Characterization of the AMP-activated protein kinase kinase from rat liver and identification of threonine 172 as the major site at which it phosphorylates AMP-activated protein kinase. J Biol Chem 1996;271:27879–87.

Herzig S, Shaw RJ. AMPK: guardian of metabolism and mitochondrial homeostasis. Nat Rev Mol Cell Biol 2018;19:121–35.

Horvath P, Aulner N, Bickle M, Davies AM, Nery ED, Ebner D, et al. Screening out irrelevant cell-based models of disease. Nat Rev Drug Discov 2016;15:751–69.

Iversen L, Johansen C, Kragballe K. Signal transduction pathways in human epidermis. Eur J Dermatol 2005;15:4–12.

Jeong HW, Kim IS. TGF-beta1 enhances betaig-h3-mediated keratinocyte cell migration through the alpha3beta1 integrin and PI3K. J Cell Biochem 2004;92:770–80.

Jin HY, Gonzalez-Martin A, Miletic AV, Lai M, Knight S, Sabouri-Ghomi M, et al. Transfection of microRNA mimics should be used with caution. Front Genet 2015;6:340.

Kahata K, Dadras MS, Moustakas A. TGF-β family signaling in epithelial differentiation and epithelial-mesenchymal transition. Cold Spring Harb Perspect Biol 2018;10:a022194.

Katiyar SK, Mantena SK, Meeran SM. Silymarin protects epidermal keratinocytes from ultraviolet radiation-induced apoptosis and DNA damage by nucleotide excision repair mechanism. PLoS One 2011;6:e21410.

Kersten S, Mandard S, Tan NS, Escher P, Metzger D, Chambon P, et al. Characterization of the fasting-induced adipose factor FIAF, a novel peroxisome proliferator-activated receptor target gene. J Biol Chem 2000;275:28488–93.

Kim M, Jeong H, Lee B, Cho Y, Yoon WK, Cho A, et al. Enrichment of Short-Chain ceramides and free fatty acids in the Skin epidermis, Liver, and Kidneys of db/db Mice, a type 2 diabetes mellitus Model. Biomol Ther (Seoul) 2019b;27:457–65.

Kim SH, Choo GS, Yoo ES, Woo JS, Han SH, Lee JH, et al. Silymarin induces inhibition of growth and apoptosis through modulation of the MAPK signaling pathway in AGS human gastric cancer cells. Oncol Rep 2019a;42:1904–14.

Kocic J, Bugarski D, Santibanez JF. SMAD3 is essential for transforming growth factor-β1-induced urokinase type plasminogen activator expression and migration in transformed keratinocytes. Eur J Cancer 2012;48:1550–7.

Kroll DJ, Shaw HS, Oberlies NH. Milk thistle nomenclature: why it matters in cancer research and pharmacokinetic studies. Integr Cancer Ther 2007;6:110–9.

Laplante M, Sabatini DM. MTOR signaling at a glance. J Cell Sci 2009;122:3589–94.

Lau PW, Guiley KZ, De N, Potter CS, Carragher B, MacRae IJ. The molecular architecture of human Dicer. Nat Struct Mol Biol 2012;19:436–40.

Lee Y, Ahn C, Han J, Choi H, Kim J, Yim J, et al. The nuclear RNase III Drosha initiates microRNA processing. Nature 2003;425:415–9.

Lemus-Diaz N, Böker KO, Rodriguez-Polo I, Mitter M, Preis J, Arlt M, et al. Dissecting miRNA gene repression on single cell level with an advanced fluorescent reporter system. Sci Rep 2017;7:45197.

Lewis RA, Li J, Allenby NEE, Errington J, Hayles J, Nurse P. Screening and purification of natural products from actinomycetes that affect the cell shape of fission yeast. J Cell Sci 2017;130:3173–85.

Li AG, Wang D, Feng XH, Wang XJ. Latent TGFbeta1 overexpression in keratinocytes results in a severe psoriasis-like skin disorder. EMBO J 2004;23:1770–81.

Li Q, Zhang D, Wang Y, Sun P, Hou X, Larner J, et al. MiR-21/Smad 7 signaling determines TGF-β1-induced CAF formation. Sci Rep 2013;3:2038.

Li W, Mu D, Song L, Zhang J, Liang J, Wang C, et al. Molecular mechanism of silymarin-induced apoptosis in a highly metastatic lung cancer cell line Anip973. Cancer Biother Radiopharm 2011a;26:317–24.

Li Y, Xu S, Mihaylova MM, Zheng B, Hou X, Jiang B, et al. AMPK phosphorylates and inhibits SREBP activity to attenuate hepatic steatosis and atherosclerosis in diet-induced insulin-resistant mice. Cell Metab 2011b;13:376–88.

Liechty C, Hu J, Zhang L, Liechty KW, Xu J. Role of microRNA-21 and its underlying mechanisms in inflammatory responses in diabetic wounds. Int J Mol Sci 2020;21:3328. 21.

Lin Q, Ma L, Liu Z, Yang Z, Wang J, Liu J, et al. Targeting microRNAs: a new action mechanism of natural compounds. Oncotarget 2017;8:15961–70.

Liu J, Valencia-Sanchez MA, Hannon GJ, Parker R. MicroRNA-dependent localization of targeted mRNAs to mammalian P-bodies. Nat Cell Biol 2005;7:719–23.

Liu Y, Li Y, Li N, Teng W, Wang M, Zhang Y, et al. TGF-β1 promotes scar fibroblasts proliferation and transdifferentiation via up-regulating MicroRNA-21. Sci Rep 2016;6:32231.

Livak KJ, Schmittgen TD. Analysis of relative gene expression data using real-time quantitative PCR and the 2(-Delta Delta C(T)) Method. Methods 2001;25:402–8.

Lowes MA, Bowcock AM, Krueger JG. Pathogenesis and therapy of psoriasis. Nature 2007;445:866–73.

Ma C, Schupp CW, Armstrong EJ, Armstrong AW. Psoriasis and dyslipidemia: a population-based study analyzing the National Health and Nutrition Examination Survey (NHANES). J Eur Acad Dermatol Venereol 2014;28:1109–12.

Man MQ, Choi EH, Schmuth M, Crumrine D, Uchida Y, Elias PM, et al. Basis for improved permeability barrier homeostasis induced by PPAR and LXR activators: liposensors stimulate lipid synthesis, lamellar body secretion, and post-secretory lipid processing. J Invest Dermatol 2006;126:386–92.

Mao-Qiang M, Fowler AJ, Schmuth M, Lau P, Chang S, Brown BE, et al. Peroxisome-proliferator-activated receptor (PPAR)-γ activation stimulates keratinocyte differentiation. J Invest Dermatol 2004;123:305–12.

Massagué J. TGF-β Signal transduction. Annu Rev Biochem 1998;67:753–91.

Massagué J. TGFβ signalling in context. Nat Rev Mol Cell Biol 2012;13:616–30.

Matsumoto K, Hashimoto K, Hashiro M, Yoshimasa H, Yoshikawa K. Modulation of growth and differentiation in normal human keratinocytes by transforming growth factor-beta. J Cell Physiol 1990;145:95–101.

McMullan R, Lax S, Robertson VH, Radford DJ, Broad S, Watt FM, et al. Keratinocyte differentiation is regulated by the Rho and ROCK signaling pathway. Curr Biol 2003;13:2185–9.

Meisgen F, Xu N, Wei T, Janson PC, Obad S, Broom O, et al. MiR-21 is up-regulated in psoriasis and suppresses T cell apoptosis. Exp Dermatol 2012;21:312–4.

Missero C, Calautti E, Eckner R, Chin J, Tsai LH, Livingston DM, et al. Involvement of the cell-cycle inhibitor Cip1/WAF1 and the E1A-associated p300 protein in terminal differentiation. Proc Natl Acad Sci USA 1995;92:5451–5.

Motta S, Monti M, Sesana S, Caputo R, Carelli S, Ghidoni R. Ceramide composition of the psoriatic scale. Biochim Biophys Acta 1993;1182:147–51.

Motta S, Monti M, Sesana S, Mellesi L, Ghidoni R, Caputo R. Abnormality of water barrier function in psoriasis. Role of ceramide fractions. Arch Dermatol 1994;130:452–6.

Mullokandov G, Baccarini A, Ruzo A, Jayaprakash AD, Tung N, Israelow B, et al. High-throughput assessment of microRNA activity and function using microRNA sensor and decoy libraries. Nat Methods 2012;9:840–6.

Nakajima K, Terao M, Takaishi M, Kataoka S, Goto-Inoue N, Setou M, et al. Barrier abnormality due to ceramide deficiency leads to psoriasiform inflammation in a mouse model. J Invest Dermatol 2013;133:2555–65.

Nestle FO, Kaplan DH, Barker J, Psoriasis. N Engl J Med 2009;361:496–509.

Newman DJ, Cragg GM. Natural products as sources of new drugs over the nearly four decades from 01/1981 to 09/2019. J Nat Prod 2020;83:770–803.

Nguyen BC, Lefort K, Mandinova A, Antonini D, Devgan V, Della Gatta G, et al. Cross-regulation between Notch and p63 in keratinocyte commitment to differentiation. Genes Dev 2006;20:1028–42.

Nofal A, Ibrahim AM, Nofal E, Gamal N, Osman S. Topical silymarin versus hydroquinone in the treatment of melasma: A comparative study. J Cosmet Dermatol 2019;18:263–70.

Ogami T, Tamura Y, Toss K, Yuki K, Morikawa M, Tsutsumi S, et al. MAB21L4 regulates the TGF-β-induced expression of target genes in epidermal keratinocytes. J Biochem 2022;171:399–410.

Pardali K, Kurisaki A, Morén A, Dijke P ten, Kardassis D, Moustakas A. Role of Smad proteins and transcription factor Sp1 in p21WAF1/Cip1 regulation by transforming growth factor-β *. J Biol Chem 2000;275:29244–56.

Pitchiaya S, Mourao MDA, Jalihal AP, Xiao L, Jiang X, Chinnaiyan AM, et al. Dynamic recruitment of single RNAs to processing bodies depends on RNA functionality. Mol Cell 2019;74:521–33.e6.

Ponec M, Weerheim A, Kempenaar J, Mommaas AM, Nugteren DH. Lipid composition of cultured human keratinocytes in relation to their differentiation. J Lipid Res 1988;29:949–61.

Ramot Y, Mastrofrancesco A, Camera E, Desreumaux P, Paus R, Picardo M. The role of PPARγ-mediated signalling in skin biology and pathology: new targets and opportunities for clinical dermatology. Exp Dermatol 2015;24:245–51.

Rendon A, Schäkel K. Psoriasis pathogenesis and treatment. Int J Mol Sci 2019;20:E1475.

Rivier M, Safonova I, Lebrun P, Griffiths CE, Ailhaud G, Michel S. Differential expression of peroxisome proliferator-activated receptor subtypes during the differentiation of human keratinocytes. J Invest Dermatol 1998;111:1116–21.

Salmerón-Manzano E, Garrido-Cardenas JA, Manzano-Agugliaro F. Worldwide research trends on medicinal plants. Int J Environ Res Public Health 2020;17:E3376.

Santibañez JF. JNK mediates TGF-beta1-induced epithelial mesenchymal transdifferentiation of mouse transformed keratinocytes. FEBS Lett 2006;580:5385–91.

Santibáñez JF, Iglesias M, Frontelo P, Martínez J, Quintanilla M. Involvement of the Ras/MAPK signaling pathway in the modulation of urokinase production and cellular invasiveness by transforming growth factor-beta(1) in transformed keratinocytes. Biochem Biophys Res Commun 2000;273: 521–7.

Schmuth M, Moosbrugger-Martinz V, Blunder S, Dubrac S. Role of PPAR, LXR, and PXR in epidermal homeostasis and inflammation. Biochim Biophys Acta 2014;1841:463–73.

Secker GA, Shortt AJ, Sampson E, Schwarz QP, Schultz GS, Daniels JT. TGFβ stimulated re-epithelialisation is regulated by CTGF and Ras/MEK/ERK signalling. Exp Cell Res 2008;314:131–42.

Sellheyer K, Bickenbach JR, Rothnagel JA, Bundman D, Longley MA, Krieg T, et al. Inhibition of skin development by overexpression of transforming growth factor beta 1 in the epidermis of transgenic mice. Proceedings of the National Academy of Sciences. Proc Natl Acad Sci USA 1993;90: 5237–41.

Shan G, Li Y, Zhang J, Li W, Szulwach KE, Duan R, et al. A small molecule enhances RNA interference and promotes microRNA processing. Nat Biotechnol 2008;26:933–40.

Simion V, Henriet E, Juric V, Aquino R, Loussouarn C, Laurent Y, et al. Intracellular trafficking and functional monitoring of miRNA delivery in glioblastoma using lipopolyplexes and the miRNA-ON RILES reporter system. J Control Release 2020;327:429–43.

Simion V, Loussouarn C, Laurent Y, Roncali L, Gosset D, Reverchon F, et al. LentiRILES, a miRNA-ON sensor system for monitoring the functionality of miRNA in cancer biology and therapy. RNA Biol 2021;18:198–214.

Simion V, Sobilo J, Clemoncon R, Natkunarajah S, Ezzine S, Abdallah F, et al. Positive radionuclide imaging of miRNA expression using RILES and the human sodium iodide symporter as reporter gene is feasible and supports a protective role of miRNA-23a in response to muscular atrophy. PLoS One 2017;12:e0177492.

Smeden J van, Bouwstra JA. Stratum corneum lipids: their role for the skin barrier function in healthy subjects and atopic dermatitis patients. Curr Probl Dermatol 2016;49:8–26.

Soleimani V, Delghandi PS, Moallem SA, Karimi G. Safety and toxicity of silymarin, the major constituent of milk thistle extract: an updated review. Phytother Res 2019;33:1627–38.

Sonkoly E, Ståhle M, Pivarcsi A. MicroRNAs: novel regulators in skin inflammation. Clin Exp Dermatol 2008;33:312–5.

Sonkoly E, Wei T, Janson PCJ, Sääf A, Lundeberg L, Tengvall-Linder M, et al. MicroRNAs: novel regulators involved in the pathogenesis of psoriasis? PLoS One 2007;2:e610.

Sukonina V, Lookene A, Olivecrona T, Olivecrona G. Angiopoietin-like protein 4 converts lipoprotein lipase to inactive monomers and modulates lipase activity in adipose tissue. Proc Natl Acad Sci USA 2006;103: 17450–5.

Svobodová A, Zdařilová A, Mališková J, Mikulková H, Walterová D, Vostalová J. Attenuation of UVA-induced damage to human keratinocytes by silymarin. J Dermatol Sci 2007;46:21–30.

Tang Y, Wallace M, Sanchez-Gurmaches J, Hsiao WY, Li H, Lee PL, et al. Adipose tissue mTORC2 regulates ChREBP-driven de novo lipogenesis and hepatic glucose metabolism. Nat Commun 2016;7:11365.

Tawada C, Kanoh H, Nakamura M, Mizutani Y, Fujisawa T, Banno Y, et al. Interferon-γ decreases ceramides with long-chain fatty acids: possible involvement in atopic dermatitis and psoriasis. J Invest Dermatol 2014;134:712–8.

Thomson DW, Pillman KA, Anderson ML, Lawrence DM, Toubia J, Goodall GJ, et al. Assessing the gene regulatory properties of Argonaute-bound small RNAs of diverse genomic origin. Nucleic Acids Res 2015;43:470–81.

Truong AB, Kretz M, Ridky TW, Kimmel R, Khavari PA. p63 regulates proliferation and differentiation of developmentally mature keratinocytes. Genes Dev 2006;20:3185–97.

van der Fits L, Mourits S, Voerman JSA, Kant M, Boon L, Laman JD, et al. Imiquimod-induced psoriasis-like skin inflammation in mice is mediated via the IL-23/IL-17 axis. J Immunol 2009;182:5836–45.

Varga T, Czimmerer Z, Nagy L. PPARs are a unique set of fatty acid regulated transcription factors controlling both lipid metabolism and inflammation. Biochim Biophys Acta 2011;1812:1007–22.

Varghese L, Agarwal C, Tyagi A, Singh RP, Agarwal R. Silibinin efficacy against human hepatocellular carcinoma. Clin Cancer Res 2005;11: 8441–8.

Vietri Rudan M, Watt FM. Mammalian epidermis: a compendium of lipid functionality. Front Physiol 2021;12:804824.

Wang J, Qiu Y, Shi NW, Zhao JN, Wang YC, Jiang H, et al. microRNA-21 mediates the TGF-β1-induced migration of keratinocytes via targeting PTEN. Eur Rev Med Pharmacol Sci 2016;20:3748–59.

Wang P, Zou F, Zhang X, Li H, Dulak A, Tomko RJ, et al. microRNA-21 negatively regulates Cdc25A and cell cycle progression in colon cancer cells. Cancer Res 2009;69:8157–65.

Wang SY, Kim H, Kwak G, Jo SD, Cho D, Yang Y, et al. Development of microRNA-21 mimic nanocarriers for the treatment of cutaneous wounds. Theranostics 2020;10:3240–53.

Wang T, Zhang L, Shi C, Sun H, Wang J, Li R, et al. TGF-β-induced miR-21 negatively regulates the antiproliferative activity but has no effect on EMT of TGF-β in HaCaT cells. Int J Biochem Cell Biol 2012;44:366–76.

Wang W, Yu X, Wu C, Jin H. IL-36γ inhibits differentiation and induces inflammation of keratinocyte via Wnt signaling pathway in psoriasis. Int J Med Sci 2017;14:1002–7.

Wang XJ, Liefer KM, Tsai S, O'Malley BW, Roop DR. Development of gene-switch transgenic mice that inducibly express transforming growth factor β1 in the epidermis. Proceedings of the National Academy of Sciences. Proc Natl Acad Sci USA 1999;96:8483–8.

Wilgus TA, Ross MS, Parrett ML, Oberyszyn TM. Topical application of a selective cyclooxygenase inhibitor suppresses UVB mediated cutaneous inflammation. Prostaglandins Other Lipid Mediat 2000;62: 367–84.

Wölfle U, Haarhaus B, Seiwerth J, Cawelius A, Schwabe K, Quirin KW, et al. The herbal bitter drug Gentiana lutea modulates lipid synthesis in human keratinocytes in vitro and in vivo. Int J Mol Sci 2017;18:18:1814.

Won D-H, Kim L-H, Jang B, Yang I-H, Kwon H-J, Jin B, et al. In vitro and in vivo anti-cancer activity of silymarin on oral cancer. Tumour biol. Tumour Biol 2018;40:1010428318776170.

Xie J, Wu W, Zheng L, Lin X, Tai Y, Wang Y, et al. Roles of MicroRNA-21 in skin wound healing: a comprehensive review. Front Pharmacol 2022;13: 828627.

Xu J, Lamouille S, Derynck R. TGF-beta-induced epithelial to mesenchymal transition. Cell Res 2009;19:156–72.

Yan L, Cao R, Liu Y, Wang L, Pan B, Lv X, et al. MiR-21-5p links epithelial-mesenchymal transition phenotype with stem-like cell signatures via AKT signaling in keloid keratinocytes. Sci Rep 2016;6:28281.

Yang CH, Yue J, Pfeffer SR, Fan M, Paulus E, Hosni-Ahmed A, et al. MicroRNA-21 promotes glioblastoma tumorigenesis by down-regulating insulin-like growth factor-binding protein-3 (IGFBP3). J Biol Chem 2014;289: 25079–87.

Yang X, Wang J, Guo SL, Fan KJ, Li J, Wang YL, et al. miR-21 promotes keratinocyte migration and re-epithelialization during wound healing. Int J Biol Sci 2011;7:685–90.

Yoshida T, Asano Y, Ui-Tei K. Modulation of microRNA processing by dicer via its associated dsRNA binding proteins. Noncoding RNA 2021;7:7:57.

Yousef H, Alhajj M, Sharma S. Anatomy, skin (integument), epidermis. In: StatPearls [Internet]. Treasure Island, FL: StatPearls Publishing; 2022.

Zhang B, Tian L, Xie J, Chen G, Wang F. Targeting miRNAs by natural products: A new way for cancer therapy. Biomed Pharmacother 2020;130: 110546.

Zhang B, Wang X, Deng J, Zheng H, Liu W, Chen S, et al. p53-dependent upregulation of miR-16-2 by sanguinarine induces cell cycle arrest and apoptosis in hepatocellular carcinoma. Cancer Lett 2019;459:50–8.

Zi X, Feyes DK, Agarwal R. Anticarcinogenic effect of a flavonoid antioxidant, silymarin, in human breast cancer cells MDA-MB 468: induction of G1 arrest through an increase in Cip1/p21 concomitant with a decrease in kinase activity of cyclin-dependent kinases and associated cyclins. Clin Cancer Res 1998a;4:1055–64.

Zi X, Grasso AW, Kung HJ, Agarwal R. A flavonoid antioxidant, silymarin, inhibits activation of erbB1 signaling and induces cyclin-dependent kinase inhibitors, G1 arrest, and anticarcinogenic effects in human prostate carcinoma DU145 cells. Cancer Res 1998b;58:1920–9.